Received: 30 November 2021 | Revised: 29 June 2022 | Accepted: 7 July 2022

DOI: 10.1002/rnc.6307

RESEARCH ARTICLE

WILEY

Sliding mode observers for robust fault estimation in linear parameter varying systems

Lejun Chen[1] | **Christopher Edwards**[2] | **Halim Alwi**[2] | **Masayuki Sato**[3] | **Shamila Nateghi**[4] | **Yuri Shtessel**[4]

[1]Department of Electronics and Electrical Engineering, University College London, London, UK

[2]College of Engineering, Mathematics & Physical Sciences, University of Exeter, Devon, UK

[3]Japan Aerospace Exploration Agency, Mitaka, Tokyo, Japan

[4]University of Alabama, Huntsville, AL, USA

Correspondence
Lejun Chen, Department of Electronics and Electrical Engineering, University College London, UK.
Email: Lejun.Chen@ucl.ac.uk

Funding information
H2020 Research Infrastructures, Grant/Award Number: 690811; Japan NEDO, Grant/Award Number: 062800

Abstract

A linear parameter varying sliding mode fault reconstruction scheme is proposed. Compared with other conventional sliding mode observer designs, the estimate emerges quite naturally from the equations governing the sliding motion, and although the process may be viewed as a filtering of the discontinuous injection, there is no phase lag introduced in the process. A semi-analytic solution to the proposed linear parameter varying sliding mode observer is first discussed. This motivates the structure of the linear matrix inequality formulation which is proposed, and clarifies the class of systems to which the approach is applicable. The linear matrix inequality problem set up minimizes the induced $\mathcal{L}_2$ gain between the fault estimate and external disturbances, whilst ensuring linear quadratic performance of the underpinning sliding motion. The proposed scheme has been validated using the Japan Aerospace Exploration Agency's Multi-Purpose Aviation Laboratory aircraft-in-the-loop platform to demonstrate the design efficacy.

KEYWORDS

aerospace, fault diagnosis, hardware-in-the-loop testing, linear parameter varying systems, sliding mode observer

1 | INTRODUCTION

This article considers the problem of unknown input estimation in linear parameter varying (LPV) systems.[1,2] The problem of unknown input estimation has a rich history in the literature, and furthermore such problems appear in many different practical aerospace engineering applications.[3-7] For many years, *fault estimation*, as a special case of unknown input estimation, has been of great interest to the fault detection and isolation (FDI) community.[8-10] Fault estimation represents a particular case of the more general fault detection and isolation problem in which an alarm should be raised at the occurrence of a fault, and its location within the system should be subsequently isolated. The fault estimation approach is more powerful in the sense that both the magnitude and "shape" of the fault are re-created via the estimation (and as such the fault estimate can often be used to directly compensate for the fault to effect fault tolerant control[11]). Unknown input estimation is also exploited in so-called disturbance compensation control.[12] Here closed loop robustness is achieved by first using an observer to estimate disturbances within the feedback loop, and then exploiting this

information to cancel the effect of the disturbance on the system outputs of interest. Another area where unknown input reconstruction is also employed is in the creation of virtual sensors. In many engineering systems certain quantities of interest cannot be directly measured—either because of physical in-accessibility, or else the absence of a sensor capable of measuring the quantity of interest directly. In these situations virtual sensors can be developed whereby other quantities are measured which, together with a model of the system capturing the interaction of the unmeasurable quantities and those which are measured, can be posed as an unknown input estimation problem.[5,13,14] Finally the fast developing area of protecting systems against cyber-attacks can also be posed in an unknown input problem framework.[15,16]

Because of the engineering applicability of the unknown input reconstruction problem for linear time invariant (LTI) systems, unsurprisingly, a rich collection of different approaches have been developed. For example the ubiquitous (Extended) Kalman filter[17,18] has been used—often involving augmenting the state-space representation with the unknown input signals considered to be states (under the assumption the rate of the change of the unknown input is small). Corless and Tu[19] developed a well cited bespoke formulation based on a linear observer formulation for LTI systems. Other more recent work by Zak and co-workers[20] also investigated this problem. In an FDI setting Stoustrup and Neimann[21] are considered to be the first to address the problem of robust fault estimation using an $\mathcal{H}_\infty$ methodology. The $\mathcal{H}_\infty$ method for fault estimation has subsequently been considered extensively in aerospace problems.[22,23] High-gain observers[24] have been presented in a number of contexts, which typically involves augmenting the states with the unknown input signal and creating an augmented system in which the unknown input is the derivative of the disturbance signals*. Many of the approaches originally developed in an LTI setting have been extended for LPV plant representations.[2] LPV systems have been widely exploited in an aerospace problem setting as a formal extension to gain scheduling. Some of the fault estimation work based on $\mathcal{H}_\infty$ methods has been extended to LPV system representations.[9] Also in recent years, LTI unknown input observers have been extended into a linear parameter varying framework[25,26] and the state affine framework.[27]

Sliding mode observers were first investigated and heralded in terms of their robustness that is, estimating the unknown internal states from measured inputs and outputs in the presence of disturbances. However in the 1990's it was demonstrated that by appropriate processing of the equivalent output error injection signal necessary to maintain sliding, the unknown input (faults) could be simultaneously estimated along with the states.[22,28,29] Subsequently this sparked interest in the use of sliding mode observers for fault detection and estimation.[30] The early work of Walcott and Zak[20] and Edwards and Spurgeon[31] consider conventional sliding mode observers and were subject to relative degree one and minimum phase conditions on the dynamical system relating the unknown input to the measurement. Work attempting to obviate these conditions appears in Reference 30. (Minimum phase and relative degree one conditions are also related to the classical constraints for linear UIOs.) The relative degree condition was completely obviated by the use of higher-order sliding mode observers/differentiators as proposed by Levant;[32] Fridman[33] combined these with a Luenberger observer framework to create a general form of unknown input observer. The ideas have also been extended to nonlinear systems.[34] Higher order sliding mode observers have been also extended to create finite time sliding mode observers.[35,36] These ideas have also been applied to various aerospace applications such as the 3-DoF helicopter,[37] a quadrotor UAV[35] and multi-sensor fusion problems.[38] Higher order sliding modes effectively address the problem of unknown input reconstruction in non-unity relative degree systems. However in sensor fault reconstruction problems, relative degree is not the primary difficulty (such problems are relative degree zero in nature). As a consequence conventional sliding mode observers can be employed and model robustness issues are addressed at the point of design. In these formulations, the unknown input signal is reconstructed via the equivalent output error injection signal.[39] Traditionally this involves the use of low pass filters. This helps remove the effects of noise but adds a phase delay to the reconstruction. The methodology presented in this article allows the fault estimate to emerge naturally from the dynamics associated with the sliding motion. As a consequence, although filtering is still involved, there is no additional phase delay introduced in the unknown input estimation signal.

In this article, the approach is applied to a sensor fault reconstruction problem. Specifically the proposed novel sliding mode observer scheme is validated using the Japan Aerospace Exploration Agency's (JAXA) Multi-Purpose Aviation Laboratory (MuPAL-α) aircraft-in-the-loop (AIL) platform, incorporating a full scaled manned aircraft and a pilot. The validation results show promising fault reconstruction performance, with and without wind/gust, in the face of various fault scenarios.

The remainder of the article is structured as follows: in Section 2, the formulation of the observer involving the synthesis of the observer gains (via an LMI optimization) and the modulation gain is discussed; the AIL platform, testing scenarios, and AIL validation results are presented in Section 3. Finally, Section 4 provides some concluding remarks.

2 | OBSERVER FORMULATION

Consider an nth order uncertain LPV system affected by a class of sensor faults modeled as

$$\begin{aligned} \dot{x} &= A(\rho)x + B(\rho)u + F(\rho)f + M(\rho)d \\ y &= Cx + Nf, \end{aligned} \tag{1}$$

where the measured output $y \in \mathbb{R}^p$ and the unknown sensor fault $f \in \mathbb{R}^q$ with $n > p > q$. The system input $u \in \mathbb{R}^m$ and the external (unknown) disturbance $d \in \mathbb{R}^k$. This lumped term is intended to capture the modeling mismatch between the nominal LPV representation in (1) and the true engineering system being monitored. Here $N \in \mathbb{R}^{p\times q}$ is the fault distribution matrix which is assumed to be rank q. In (1) u and y are measurable, and it is assumed the output distribution matrix C has full row rank. Also assume that both f, d and $\dot{f}$ are bounded and that specifically $\|f\| < k_f$, $\|d\| < k_d$ and $\|\dot{f}\| < l_f$ where the positive scalars k_f, k_d and l_f are known. In this article, it is assumed the time-varying, differentiable scheduling parameter $\rho(t) \in \Omega \subset \mathbb{R}^r$ is known accurately and belongs to a compact set Ω.

Assumption 1. It is assumed that $(A(\rho), C)$ is quadratically observable.

Remark 1. In analytic fault redundancy approaches the fidelity of model about which the observer is designed is important. Improved modeling accuracy helps minimize false alarms and improves fault reconstruction accuracy. The move from LTI to LPV models is a natural way to achieve this—especially in aerospace applications.

Remark 2. In this article it is assumed $\rho(t)$ is perfectly known. This is a common assumption in the LPV literature. However, some researchers have investigated how imperfect knowledge of $\rho(t)$ affects the performance of observers.[40] These also include a class of LPV SMOs.[41,42]

Consider the application of a nonsingular (output) scaling matrix $Q \in \mathbb{R}^{p\times p}$ chosen such that

$$QN = \begin{bmatrix} 0 \\ N_2 \end{bmatrix}, \tag{2}$$

where $N_2 \in \mathbb{R}^{q\times q}$ is nonsingular. From the rank assumption on N, the matrix Q in (2) can be obtained by Gaussian elimination (or QR decomposition).

Since the output distribution matrix $\overline{C} = QC$ associated with the scaled outputs is also full row rank there always exists a nonsingular square matrix $T_c \in \mathbb{R}^{n\times n}$ and the change of coordinates $x \mapsto T_c x$ that creates a system representation in which the output distribution matrix has the form $\begin{bmatrix} 0 & I_p \end{bmatrix}$. Hence, w.l.o.g it is assumed the representation in (1) is such that

$$\overline{C} = QC = \begin{bmatrix} 0 & I_p \end{bmatrix}.$$

Define $\overline{y}$ as the scaled outputs y according to $\overline{y} = Qy$ and partition $\overline{y}$ as $\text{col}(\overline{y}_1, \overline{y}_2)$ then

$$\begin{aligned} \overline{y}_1 &= C_1 x \\ \overline{y}_2 &= C_2 x + N_2 f, \end{aligned} \tag{3}$$

where $C_1 = \begin{bmatrix} 0 & I_{p-q} & 0 \end{bmatrix}$ and $C_2 = \begin{bmatrix} 0 & I_q \end{bmatrix}$.

The objective is to develop an LPV observer for the system in (1) based on the scaled outputs $\overline{y}_1$ and $\overline{y}_2$ of the form

$$\dot{z} = A(\rho)z + B(\rho)u + G_1(\rho)(\overline{y}_1 - C_1 z) + G_2(\rho)(\overline{y}_2 - C_2 z) - G_n \nu, \tag{4}$$

where the injection signal ν is a function of $\overline{y}_2 - C_2 z$. The aim is to induce sliding on $\overline{y}_2 - C_2 z$ for the purpose of estimating the fault signal f. The objective is to minimize the effect of the plant model mismatch by minimizing the effect of d in (1) on the fault reconstruction error in an induced $\mathcal{L}_2$ norm sense.

The next section develops a possible analytic solution to give an insight into the problem, and to provide the necessary conditions under which the problem is solvable.

2.1 | An analytic solution

Here it is assumed that $(A(\rho), C)$ is quadratically observable (Assumption 1). Define a further change of coordinates $(x_1, x_2) \mapsto (\bar{x}_1, x_2)$ according to $\bar{x}_1 = x_1 + Lx_2$ where $L \in \mathbb{R}^{(n-p)\times p}$. As argued in Reference 43 there exist choices of L such that the system can be written as

$$\dot{\bar{x}}_1 = \bar{A}_{11}(\rho)\bar{x}_1 + \bar{A}_{12}(\rho)\bar{x}_2 + \overline{B}_1(\rho)u + \overline{F}_1(\rho)f + \overline{M}_1(\rho)d, \tag{5}$$

$$\dot{\bar{x}}_2 = \bar{A}_{21}(\rho)\bar{x}_1 + \bar{A}_{22}(\rho)\bar{x}_2 + \overline{B}_2(\rho)u + \overline{F}_2(\rho)f + \overline{M}_2(\rho)d, \tag{6}$$

where $\bar{A}_{11}(\rho)$ is quadratically stable and $\bar{x}_2 = \bar{y}$.

Define $\bar{x}_2 = \mathrm{col}(\bar{x}_{21}, \bar{x}_{22})$, where $\bar{x}_{21} \in \mathbb{R}^{p-q}$ and $\bar{x}_{22} \in \mathbb{R}^q$, then the scaled outputs are

$$\bar{y}_1 = \bar{x}_{21}, \tag{7}$$

$$\bar{y}_2 = \bar{x}_{22} + N_2 f. \tag{8}$$

Note by definition $\bar{x}_{21}$ is a known quantity (because it is obtained from $\bar{y}$) and it is free from corruption that is, independent of f. Consequently the system in (5)-(6) can be written in partitioned form as

$$\dot{\bar{x}}_1 = \bar{A}_{11}(\rho)\bar{x}_1 + \bar{A}_{121}(\rho)\bar{x}_{21} + \bar{A}_{122}(\rho)\bar{x}_{22} + \overline{B}_1(\rho)u + \overline{F}_1(\rho)f + \overline{M}_1(\rho)d, \tag{9}$$

$$\dot{\bar{x}}_{21} = \bar{A}_{211}(\rho)\bar{x}_1 + \bar{A}_{221}(\rho)\bar{x}_{21} + \bar{A}_{222}(\rho)\bar{x}_{22} + \overline{B}_{21}(\rho)u + \overline{F}_{21}(\rho)f + \overline{M}_{21}(\rho)d, \tag{10}$$

$$\dot{\bar{x}}_{22} = \bar{A}_{212}(\rho)\bar{x}_1 + \bar{A}_{223}(\rho)\bar{x}_{21} + \bar{A}_{224}(\rho)\bar{x}_{22} + \overline{B}_{22}(\rho)u + \overline{F}_{22}(\rho)f + \overline{M}_{22}(\rho)d, \tag{11}$$

for appropriate choices of submatrices. For notational convenience write (9)–(11) as

$$\dot{\bar{x}} = \bar{A}(\rho)\bar{x} + \overline{B}(\rho)u + \overline{F}(\rho)f + \overline{M}(\rho)d \tag{12}$$

and

$$\bar{y}_1 = \overline{C}_1\bar{x}, \tag{13}$$

$$\bar{y}_2 = \overline{C}_2\bar{x} + N_2 f, \tag{14}$$

where $\overline{C}_1 = C_1$ and $\overline{C}_2 = C_2$. Define a (sliding mode) observer for the system (12)–(14) based on (4), and taking account of the change of coordinates, as

$$\dot{\bar{z}} = \bar{A}(\rho)\bar{z} + \overline{B}(\rho)u + \overline{G}_1(\rho)(\bar{y}_1 - \bar{z}_{21}) + \overline{G}_2(\rho)(\bar{y}_2 - \bar{z}_{22}) - \overline{G}_n\nu, \tag{15}$$

where $\bar{z} = \mathrm{col}(\bar{z}_1, \bar{z}_{21}, \bar{z}_{22})$ is partitioned conformally with the partition of $\bar{x}$ in (9)–(11). The signal ν in (15) represents a nonlinear injection signal depending on $(\bar{y}_2 - \bar{z}_{22})$ whose purpose is to produce a sliding motion in finite time in the estimation error space.

Define the observer gain matrix in (15) associated with ν as

$$\overline{G}_n = \begin{bmatrix} 0 \\ 0 \\ I_q \end{bmatrix} \tag{16}$$

Also define $\overline{G}_1(\rho)$ and $\overline{G}_2(\rho)$ as

$$\overline{G}_1(\rho) = \begin{bmatrix} \bar{A}_{121}(\rho) \\ \bar{A}_{221}(\rho) - A^s_{22} \\ 0 \end{bmatrix} \tag{17}$$

and

$$\overline{G}_2(\rho) = \begin{bmatrix} \bar{A}_{122}(\rho) \\ \bar{A}_{222}(\rho) \\ \bar{A}_{224}(\rho) - A^s_{33} \end{bmatrix}, \tag{18}$$

where $A^s_{22} \in \mathbb{R}^{(p-q)\times(p-q)}$ and $A^s_{33} \in \mathbb{R}^{q\times q}$ are Hurwitz matrices which constitute design freedom. This will be shown to represent a semi-analytic solution to the problem. In particular, assume that A^s_{33} is symmetric negative definite. The injection signal in (15) is defined as

$$\nu = -\mathcal{K}(t)\frac{\bar{y}_2 - \bar{z}_{22}}{\|\bar{y}_2 - \bar{z}_{22}\|}, \tag{19}$$

where the so-called modulation gain $\mathcal{K}(t)$ will be defined explicitly later.

Define $\bar{e} = \bar{x} - \bar{z}$ then it follows $\bar{e} = \text{col}(\bar{e}_1, \bar{e}_{21}, \bar{e}_{22})$ where $\bar{e}_1 = \bar{x}_1 - \bar{z}_1$, $\bar{e}_{21} = \bar{x}_{21} - \bar{z}_{21}$, $\bar{e}_{22} = \bar{x}_{22} - \bar{z}_{22}$. In particular

$$\bar{y}_2 - \bar{z}_{22} = \bar{x}_{22} + N_2 f - \bar{z}_{22} = \bar{e}_{22} + N_2 f \tag{20}$$

and then substituting from (9)–(11) and (15), it follows that

$$\begin{bmatrix} \dot{\bar{e}}_1 \\ \dot{\bar{e}}_{21} \\ \dot{\bar{e}}_{22} \end{bmatrix} = \begin{bmatrix} \bar{A}_{11}(\rho) & 0 & 0 \\ \bar{A}_{211}(\rho) & A^s_{22} & 0 \\ \bar{A}_{212}(\rho) & \bar{A}_{223}(\rho) & A^s_{33} \end{bmatrix} \begin{bmatrix} \bar{e}_1 \\ \bar{e}_{21} \\ \bar{e}_{22} \end{bmatrix} - \begin{bmatrix} \bar{A}_{122}(\rho) \\ \bar{A}_{222}(\rho) \\ \bar{A}_{224}(\rho) - A^s_{33} \end{bmatrix} N_2 f + \begin{bmatrix} \overline{F}_1(\rho) \\ \overline{F}_{21}(\rho) \\ \overline{F}_{22}(\rho) \end{bmatrix} f + \begin{bmatrix} \overline{M}_1(\rho) \\ \overline{M}_{21}(\rho) \\ \overline{M}_{22}(\rho) \end{bmatrix} d + \begin{bmatrix} 0 \\ 0 \\ I_q \end{bmatrix} \nu. \tag{21}$$

Assuming ν can be selected to enforce sliding, during sliding, $e_{y_2} = \bar{y}_2 - \bar{z}_{22} \equiv 0$. It follows from (20) that $\bar{e}_{22} = -N_2 f$. From (21), the sliding motion is determined by

$$\dot{\bar{e}}_{11} = \begin{bmatrix} \bar{A}_{11}(\rho) & 0 \\ \bar{A}_{211}(\rho) & A^s_{22} \end{bmatrix} \bar{e}_{11} - \begin{bmatrix} \bar{A}_{122}(\rho) - \overline{F}_1(\rho)N_2^{-1} \\ \bar{A}_{222}(\rho) - \overline{F}_{21}(\rho)N_2^{-1} \end{bmatrix} N_2 f + \begin{bmatrix} \overline{M}_1(\rho) \\ \overline{M}_{21}(\rho) \end{bmatrix} d, \tag{22}$$

where $\bar{e}_{11} = \text{col}(\bar{e}_1, \bar{e}_{21})$. During sliding $e_{y_2} = \dot{e}_{y_2} = 0$ so consequently from the last row of (21)

$$0 = \begin{bmatrix} \bar{A}_{212}(\rho) & \bar{A}_{223}(\rho) \end{bmatrix} \bar{e}_{11} - (\bar{A}_{224}(\rho) - \overline{F}_{22}(\rho)N_2^{-1})N_2 f + N_2 \dot{f} + \overline{M}_{22}(\rho)d + \nu_{eq}, \tag{23}$$

since $\dot{\bar{e}}_{22} = -N_2 \dot{f}$ where ν_{eq} is the equivalent output error injection[39] necessary to maintain sliding.

Defining $\bar{f} = -N_2 f$ it follows that the equations above can be written as

$$\begin{bmatrix} \dot{\bar{e}}_1 \\ \dot{\bar{e}}_{21} \\ \dot{\bar{f}} \end{bmatrix} = \underbrace{\begin{bmatrix} \bar{A}_{11}(\rho) & 0 & \bar{A}_{122}(\rho) - \overline{F}_1(\rho)N_2^{-1} \\ \bar{A}_{211}(\rho) & A^s_{22} & \bar{A}_{222}(\rho) - \overline{F}_{21}(\rho)N_2^{-1} \\ \bar{A}_{212}(\rho) & \bar{A}_{223}(\rho) & \bar{A}_{224}(\rho) - \overline{F}_{22}(\rho)N_2^{-1} \end{bmatrix}}_{\bar{A}_0(\rho)} \begin{bmatrix} \bar{e}_1 \\ \bar{e}_{21} \\ \bar{f} \end{bmatrix} + \underbrace{\begin{bmatrix} 0 \\ 0 \\ I_q \end{bmatrix}}_{\overline{B}_0(\rho)} \nu_{eq} + \underbrace{\begin{bmatrix} \overline{M}_1(\rho) \\ \overline{M}_{21}(\rho) \\ \overline{M}_{22}(\rho) \end{bmatrix}}_{\overline{M}_0(\rho)} d \tag{24}$$

and that

$$f = \underbrace{\begin{bmatrix} 0 & 0 & -N_2^{-1} \end{bmatrix}}_{\overline{C}_0} \begin{bmatrix} \bar{e}_1 \\ \bar{e}_{21} \\ \overline{f} \end{bmatrix}. \tag{25}$$

Define

$$\hat{f} = \mathbf{W}(\rho) v_{eq}, \tag{26}$$

where in the notation of Reference 2

$$\mathbf{W}(\rho) := \left[\begin{array}{c|c} \bar{A}_0(\rho) & \bar{B}_0(\rho) \\ \hline \bar{C}_0 & 0 \end{array}\right], \tag{27}$$

that is, from filtering the discontinuous injection v_{eq} through the operator $\mathbf{W}(\rho)$. In the situation when $d = 0$ in (24) and $\mathbf{W}(\rho)$ (which is necessary for fault estimation), then $\hat{f} = f$ holds for all $\rho \in \Omega$. The stability of the $\mathbf{W}(\rho)$ is ensured during the design process which will be discussed in the sequel.

Remark 3. Note that $\hat{f}$ is a continuous signal as it emerges from $\mathbf{W}(\rho)$ despite the fact that v_{eq} is discontinuous. Critically (26) may be viewed as an explicit way of precisely designing a low pass filter to extract the equivalent injection (in this case $\hat{f}$). Here 1st order SMOs are being employed but a continuous estimate $\hat{f}$ is obtained. Further, there is no artificially (or additionally) implemented filter to formally extract the equivalent output error injection which is used to create the estimate $\hat{f}$.

More generally, in the practical situation where $d \neq 0$, from (24) and (25), the signals d and the fault estimation error $f - \hat{f}$ are connected via the operator $\mathbf{H}(\rho)$: specifically

$$f - \hat{f} = \mathbf{H}(\rho) d \quad \forall \rho \in \Omega, \tag{28}$$

where

$$\mathbf{H}(\rho) := \left[\begin{array}{c|c} \bar{A}_0(\rho) & \bar{M}_0(\rho) \\ \hline \bar{C}_0 & 0 \end{array}\right]. \tag{29}$$

Note that in (27) and (29), the dynamics are both governed by

$$\bar{A}_0(\rho) = \bar{A}(\rho) - \overline{F}(\rho) N_2^{-1} \overline{C}_2 - \overline{G}_1(\rho) \overline{C}_1, \tag{30}$$

where $\bar{A}(\rho)$, $\overline{F}(\rho)$, $\overline{C}_1$, and $\overline{C}_2$ are defined in (12)–(14). If $\bar{A}_0(\rho)$ is (quadratically) stable for all $\rho \in \Omega$ and $d \equiv 0$, then perfect reconstruction of f is achieved asymptotically by $\hat{f}$, despite nonzero initial conditions and changes in operating conditions (i.e., changes in $\rho(t)$).

Remark 4. Theoretically once the effects of any initial state estimation error have decayed, $\hat{f} \to f$ and so there is no phase delay between $\hat{f}$ and f. This is in contrast to previously proposed schemes where $\hat{f}$ is extracted from the discontinuous injection signal via low pass filtering which results in bandwidths above which phase distortion becomes inevitable. Of course in a practical engineering situation, other unavoidable elements such as discretization, the properties of the hardware A/D and D/A employed to implement the FDI schemes, and latency in the calculations and so forth. will contribute a delay (which will not be mitigated in this proposed approach).

If $\bar{A}_0(\rho)$ is quadratically stable for all $\rho \in \Omega$, $\mathbf{W}(\rho)$ and $\mathbf{H}(\rho)$ can be considered as stable low pass filters. For the purpose of inducing robustness of the fault estimation error $f - \hat{f}$ against the effect of the external disturbance d, the design freedom in the observer given by L needs to be chosen to minimize the induced $\mathcal{L}_2$ norm of $\mathbf{H}(\rho)$ in (29). Notice that the operators $\mathbf{H}(\rho)$ and $\mathbf{W}(\rho)$ can be realized in the original coordinates of (1)–(3) as

$$\mathbf{W}(\rho) = \left[\begin{array}{c|c} A_0(\rho) & \bar{B}_0(\rho) \\ \hline C_0 & 0 \end{array}\right] \text{ and } \mathbf{H}(\rho) = \left[\begin{array}{c|c} A_0(\rho) & M(\rho) \\ \hline C_0 & 0 \end{array}\right],$$

where $A_0(\rho) = A(\rho) - F(\rho)N_2^{-1}\overline{C}_2 - G_1(\rho)\overline{C}_1$, the gain

$$G_1(\rho) = \begin{bmatrix} I_{n-p} & -L \\ 0 & I_p \end{bmatrix} \overline{G}_1(\rho)$$

and $F(\rho)$, $M(\rho)$ are defined in (1).

A linear matrix inequality (LMI) based approach will be presented in the next section to synthesize the observer gains numerically.

2.2 | Synthesis of the observer gains

The previous section developed insight into the necessary conditions for developing the observer in (4). Write the system in (1) in the form

$$\dot{x}_1 = A_{11}(\rho)x_1 + A_{12}(\rho)x_2 + B_1(\rho)u + F_1(\rho)f + M_1(\rho)d, \tag{31}$$

$$\dot{x}_2 = A_{21}(\rho)x_1 + A_{22}(\rho)x_2 + B_2(\rho)u + F_2(\rho)f + M_2(\rho)d, \tag{32}$$

where $A_{11}(\rho) \in \mathbb{R}^{(n-q)\times(n-q)}$ and $A_{22}(\rho) \in \mathbb{R}^{q\times q}$. (Note this $x = \text{col}(x_1, x_2)$ partition is of different dimension to the one in Section 2.1 and independent of the developments in that section.) The scaled outputs

$$y = \begin{bmatrix} 0 & I_p \end{bmatrix} x + \begin{bmatrix} 0 \\ N_2 \end{bmatrix} f = \left[\begin{array}{cc|c} 0 & I_{p-q} & 0 \\ 0 & 0 & I_q \end{array}\right] x + \begin{bmatrix} 0 \\ N_2 \end{bmatrix} f = \begin{bmatrix} C_1 \\ C_2 \end{bmatrix} x + \begin{bmatrix} 0 \\ N_2 \end{bmatrix} f = \begin{bmatrix} C_{11} & 0 \\ 0 & I_q \end{bmatrix} \begin{bmatrix} x_1 \\ x_2 \end{bmatrix} + \begin{bmatrix} 0 \\ N_2 \end{bmatrix} f. \tag{33}$$

This section will reverse-engineer the choice of observer gains $G_1(\rho)$ and G_n, assuming $G_1(\rho)$ in (4) has been chosen so that

$$A_0(\rho) = A(\rho) - F(\rho)N_2^{-1}C_2 - G_1(\rho)C_1 \tag{34}$$

is quadratically stable. This development starts in the original coordinate system based on the scaled outputs $\bar{y}$. For this approach to be applicable, the pair $(A(\rho) - F(\rho)N_2^{-1}C_2, C_1)$ must be detectable. An insight into this is given in the Appendix A.

Assuming the design freedom $G_1(\rho)$ has been chosen so that $A_0(\rho)$ in (34) is quadratically stable and that the corresponding Lyapunov function[†] is

$$V(x) = x^T P x \tag{35}$$

in particular

$$PA_0(\rho) + A_0^T(\rho)P < 0. \tag{36}$$

Decompose the s.p.d matrix P in (36) as

$$P := \begin{bmatrix} P_{11} & P_{12} \\ P_{12}^T & P_{22} \end{bmatrix}, \tag{37}$$

where $P_{22} \in \mathbb{R}^{q\times q}$, then define a change of coordinates matrix

$$T := \begin{bmatrix} I & P_{11}^{-1}P_{12} \\ 0 & I \end{bmatrix} \tag{38}$$

and let $\check{x} = Tx$. The matrix P_{11} is guaranteed to be invertible since P is s.p.d. In the new $\check{x}$ coordinates

$$V = \check{x}^T (T^{-1})^T P T^{-1} \check{x} = \check{x}^T \check{P} \check{x}, \tag{39}$$

where

$$\check{P} := (T^{-1})^T P T^{-1} = \begin{bmatrix} P_{11} & 0 \\ 0 & P_{22} - P_{12}^T P_{11}^{-1} P_{12} \end{bmatrix} \tag{40}$$

and therefore has block diagonal form. Define

$$\check{A}_0(\rho) = TA_0(\rho)T^{-1} = \check{A}(\rho) - \check{F}(\rho)N_2^{-1}\check{C}_2 - \check{G}_1(\rho)\check{C}_1, \tag{41}$$

where $\check{A}(\rho) = TA(\rho)T^{-1}$, $\check{F}(\rho) = TF(\rho)$, $\check{C}_1 = C_1T^{-1}$, $\check{G}_1(\rho) = TG_1(\rho)$, and $\check{C}_2 = C_2T^{-1}$, where specifically from (33)

$$\check{C}_1 = \begin{bmatrix} C_{11} & -C_{11}P_{11}^{-1}P_{12} \end{bmatrix} \quad \text{and} \quad \check{C}_2 = \begin{bmatrix} 0 & I_q \end{bmatrix} \tag{42}$$

and

$$\check{A}(\rho) = \begin{bmatrix} A_{11}(\rho) + P_{11}^{-1}P_{12}A_{21}(\rho) & * \\ A_{21}(\rho) & * \end{bmatrix}, \tag{43}$$

where $A_{11}(\rho)$ and $A_{21}(\rho)$ are defined in (31)–(32) and $*$ denotes the block element of no interest. Furthermore if $G_1(\rho) = \begin{bmatrix} G_{11}^T(\rho) & G_{12}^T(\rho) \end{bmatrix}^T$ then

$$\check{G}_1(\rho) = \begin{bmatrix} G_{11}(\rho) + P_{11}^{-1}P_{12}G_{12}(\rho) \\ G_{12}(\rho) \end{bmatrix} \tag{44}$$

and it follows from the structure of $\check{C}_2$ that

$$\check{A}_0(\rho) = \begin{bmatrix} A_{11}(\rho) + P_{11}^{-1}P_{12}A_{21}(\rho) - G_{11}(\rho)C_{11} - P_{11}^{-1}P_{12}G_{12}(\rho)C_{11} & * \\ * & * \end{bmatrix}. \tag{45}$$

Since $\check{P}$ in (40) is block diagonal and

$$\check{P}\check{A}_0(\rho) + \check{A}_0^T(\rho)\check{P} < 0, \tag{46}$$

it follows the top left sub-block of $\check{P}\check{A}_0(\rho) + \check{A}_0^T(\rho)\check{P}$ is negative definite, that is,

$$\begin{aligned} &P_{11}\left(A_{11}(\rho) + P_{11}^{-1}P_{12}A_{21}(\rho) - G_{11}(\rho)C_{11} - P_{11}^{-1}P_{12}G_{12}(\rho)C_{11}\right) \\ &\quad + \left(A_{11}(\rho) + P_{11}^{-1}P_{12}A_{21}(\rho) - G_{11}(\rho)C_{11} - P_{11}^{-1}P_{12}G_{12}(\rho)C_{11}\right)^T P_{11} < 0 \end{aligned} \tag{47}$$

it follows that

$$\check{A}(\rho) - \check{G}_1(\rho)\check{C}_1 = \begin{bmatrix} \check{A}_{11}(\rho) & \check{A}_{12}(\rho) \\ \check{A}_{21}(\rho) & \check{A}_{22}(\rho) \end{bmatrix}, \tag{48}$$

where in particular $\breve{A}_{11}(\rho) = A_{11}(\rho) + P_{11}^{-1}P_{12}A_{21}(\rho) - G_{11}(\rho)C_{11} - P_{11}^{-1}P_{12}G_{12}(\rho)C_{11}$ is quadratically stable.

Now consider the observer (in the $\breve{x}$ coordinates) as

$$\dot{\breve{z}} = \breve{A}(\rho)\breve{z} + \breve{B}(\rho)u + \breve{G}_1(\rho)(\bar{y}_1 - \breve{C}_1\breve{z}) + \breve{G}_2(\rho)(\bar{y}_2 - \breve{C}_2\breve{z}) - \breve{G}_n\nu, \tag{49}$$

where $\breve{B}(\rho) = TB(\rho)$ and define

$$\breve{G}_n = \begin{bmatrix} 0 \\ I_q \end{bmatrix} \quad \text{and} \quad \breve{G}_2(\rho) = \begin{bmatrix} \breve{A}_{12}(\rho) \\ \breve{A}_{22}(\rho) - \breve{A}_{22}^* \end{bmatrix}. \tag{50}$$

Then in the error coordinates $\breve{e} = \breve{x} - \breve{z}$ if $\breve{e} = \text{col}(\breve{e}_1 \quad \breve{e}_2)$ the error system

$$\begin{aligned} \dot{\breve{e}} &= (\breve{A}(\rho) - \breve{G}_1(\rho)\breve{C}_1)\breve{e} - \breve{G}_2(\rho)(\breve{e}_2 + N_2 f) + \breve{F}(\rho)f + \breve{G}_n\nu + \breve{M}(\rho)d \\ &= \begin{bmatrix} \breve{A}_{11}(\rho) & 0 \\ \breve{A}_{21}(\rho) & \breve{A}_{22}^* \end{bmatrix} \begin{bmatrix} \breve{e}_1 \\ \breve{e}_2 \end{bmatrix} - \begin{bmatrix} \breve{A}_{12}(\rho) - \breve{F}_1(\rho)N_2^{-1} \\ \breve{A}_{22}(\rho) - \breve{A}_{22}^* - \breve{F}_2(\rho)N_2^{-1} \end{bmatrix} N_2 f + \begin{bmatrix} 0 \\ I_q \end{bmatrix} \nu + \begin{bmatrix} \breve{M}_1(\rho) \\ \breve{M}_2(\rho) \end{bmatrix} d, \end{aligned} \tag{51}$$

where $\breve{M}(\rho) = TM(\rho)$. Note that the sliding motion is governed by the system matrix $\breve{A}_{11}(\rho)$ which is guaranteed to be quadratically stable from (47).

Define $Y(\rho) = PG_1(\rho)$. Then if $Y(\rho) = \begin{bmatrix} Y_1^T(\rho) & Y_2^T(\rho) \end{bmatrix}^T$, it can be checked that

$$Y_1(\rho) = P_{11}G_{11}(\rho) + P_{12}G_{12}(\rho), \tag{52}$$

It follows from (47) that the system matrix $\breve{A}_{11}(\rho)$ governing sliding satisfies

$$P_{11}\breve{A}_{11}(\rho) + \breve{A}_{11}^T(\rho)P_{11} = P_{11}A_{11}(\rho) + A_{11}^T(\rho)P_{11} + P_{12}A_{21}(\rho) + A_{21}^T(\rho)P_{12}^T - Y_1(\rho)C_{11} - C_{11}^T Y_1^T(\rho). \tag{53}$$

To allow tuning of the performance during the sliding mode, consider the matrix inequality

$$P_{11}A_{11}(\rho) + P_{12}A_{21}(\rho) + A_{11}^T(\rho)P_{11} + A_{21}^T(\rho)P_{12}^T - Y_1(\rho)C_{11} - C_{11}^T Y_1^T(\rho) + P_{12}W_1P_{12}^T + P_{11}W_2P_{11}^T < 0, \tag{54}$$

where W_1 and W_2 are s.p.d matrices. Clearly if (54) is satisfied then (47) holds. Using the Schur complement, (54) is equivalent to

$$\begin{bmatrix} -Y_1(\rho)C_{11} - C_{11}^T Y_1^T(\rho) + P_{11}A_{11}(\rho) + P_{12}A_{21}(\rho) + A_{11}^T(\rho)P_{11} + A_{21}^T(\rho)P_{12}^T & P_{12} & P_{11} \\ * & -W_1^{-1} & 0 \\ * & * & -W_2^{-1} \end{bmatrix} < 0. \tag{55}$$

For given designer selected weights W_1 and W_2, part of the synthesis can be formulated as the LMI problem

$$\min_{P_{11}, P_{12}, Y_1(\rho)} \text{tr}(P_{11}^{-1}) \quad \text{subject to} \quad (55). \tag{56}$$

This has the form of an LQG observer design problem for the fictitious pair $(A_{11}(\rho), A_{21}(\rho))$ for a specific choice of cost function involving the weights W_1 and W_2. The formulation can also be viewed as the natural dual of the commonly exploited quadratic cost approach for sliding mode control hyperplane design.[39,44]

The other design objective is to minimize the induced $\mathcal{L}_2$ norm of $\mathbf{H}(\rho)$ from (29). Minimizing the $\mathcal{L}_2$ gain of $\mathbf{H}(\rho)$ can also be cast as an LMI problem

$$\min_{P, Y(\rho)} \gamma \quad \text{subject to} \quad \begin{bmatrix} PA(\rho) - PF(\rho)N_2^{-1}C_2 - Y(\rho)C_1 + (*) & PM_0(\rho) & C_0^T \\ * & -\gamma I & 0 \\ * & * & -\gamma I, \end{bmatrix} < 0, \tag{57}$$

where $Y(\rho) = PG_1(\rho)$ as defined earlier, and γ denotes an upper bound on the induced $\mathcal{L}_2$ norm of $\mathbf{H}(\rho)$.

The overall design problem can be cast as

$$\min_{P,Y(\rho)} \alpha_1 \text{tr}(P_{11}^{-1}) + \alpha_2 \gamma \quad \text{subject to} \quad (55) \quad \text{and} \quad (57),$$

where α_1 and α_2 are scalar weightings. This process synthesizes the gain $G_1(\rho)$ directly. From the s.p.d matrix P, the components P_{11} and P_{12} can be identified. This specifies the matrix T in (38) and therefore from (51)

$$G_2(\rho) = T^{-1}\breve{G}_2(\rho) \quad \text{and} \quad G_n = T^{-1}\begin{bmatrix} 0 \\ I_q \end{bmatrix}. \tag{58}$$

LPV systems admit various representations, such as the polytopic/affine LPV representation,[45] the gridding-based LPV representation synthesis[2,46] and the multiplier-based linear fractional transformation (LFT) representation.[47,48] To solve (55), (57), and (58) tractably involving a finite number of LMIs "separating" the parameter-dependent system matrices and the Lyapunov matrix, here the following concession is introduced:

Assumption 2. It is assumed that $A(\rho)$, $F(\rho)$, and $M(\rho)$ depend affinely on ρ. In particular

$$A(\rho) = A_{p,0} + A_{p,1}\rho_2 + \cdots + A_{p,r}\rho_r, \tag{59}$$

where the parameter ρ_i is the ith component of ρ.

Using the vertex property discussed in Reference 45, the LMIs in (55) and (57) can be converted into a polytopic form and the synthesis of the observer gain $G_1(\rho)$ and the analysis of the design problem in (58) is undertaken only at the vertices of the polytope.

Remark 5. The above analysis is based on the establishment of a (fixed) quadratic Lyapunov function in (35). This introduces conservatism but avoids a situation in which an infinite number of matrix inequalities need to be solved.

The choice of the modulation gain to guarantee sliding is discussed in the next subsection.

2.3 | Design of the modulation gain

To develop a theory for selecting the modulation gains to enforce sliding in (51), consider the signal

$$\phi = \breve{A}_{21}(\rho)\breve{e}_1 - (\breve{A}_{22}(\rho) - \breve{F}_2(\rho)N_2^{-1})N_2 f + \breve{M}_2(\rho)d, \tag{60}$$

together with the dynamics from (51)

$$\dot{\breve{e}}_1 = \breve{A}_{11}(\rho)\breve{e}_1 - (\breve{A}_{12}(\rho) - \breve{F}_1(\rho)N_2^{-1})N_2 f + \breve{M}_1(\rho)d. \tag{61}$$

Let $w = \begin{bmatrix} f^T & d^T \end{bmatrix}^T$, then the operator $\mathbf{G}_\phi(s)$ mapping $w \mapsto \phi$ given by (61) and (60) is quadratically stable. Therefore since by assumption $\|d(t)\| < k_d$ and $\|f(t)\| < k_f$, for any initial condition $\breve{e}_1(0)$ at time $t = 0$, in finite time t_0, there exist positive scalars α_0, m_1, m_2 and m_3 such that

$$\|\phi(t)\| \leq m_1 e^{-\alpha_0 t} + m_2 \int_0^t e^{-\alpha_0(t-\tau)}(k_d + k_f)d\tau + m_3(k_d + k_f), \tag{62}$$

for all $t \geq t_0$.[24] The scalars α_0, m_1, m_2, and m_3 will now be used in the definition of the modulation gain.

Proposition 1. *By choosing the modulation gain in (19) according to*

$$\mathcal{K}(t) = m_1 e^{-\alpha_0 t} + m_2 \int_0^t e^{-\alpha_0(t-\tau)}(k_d + k_f)d\tau + m_3(k_d + k_f) + \|N_2\|l_f + \eta, \tag{63}$$

where η is a positive design scalar, a sliding motion on $\bar{y}_2 - \bar{z}_{22} = 0$ is guaranteed in finite time.

Proof. Define the output estimation error $e_{y_2} := \bar{y}_2 - \bar{z}_{22}$. Using the fact that $e_{y_2} = \check{e}_2 + N_2 f$ and it is easy to verify from (51)

$$\dot{e}_{y_2} = \check{A}_{21}(\rho)\check{e}_1 - (\check{A}_{22}(\rho) - \check{A}^*_{22} - \check{F}_2(\rho)N_2^{-1})N_2 f + \check{A}^*_{22}\check{e}_2 + N_2\dot{f} + \check{M}_2(\rho)d + \nu \tag{64}$$

$$= \check{A}_{21}(\rho)\check{e}_1 - (\check{A}_{22}(\rho) - \check{F}_2(\rho)N_2^{-1})N_2 f + \check{A}^*_{22}e_{y_2} + N_2\dot{f} + \check{M}_2(\rho)d + \nu \tag{65}$$

and therefore

$$\dot{e}_{y_2} = \check{A}^*_{22}e_{y_2} + \phi + N_2\dot{f} + \nu,$$

where ϕ is defined in (60). Since $\check{A}^*_{22}$ is symmetric negative definite, for all $t \geq t_0$

$$e^T_{y_2}\dot{e}_{y_2} \leq e^T_{y_2}\phi + e^T_{y_2}N_2\dot{f} - \mathcal{K}(t)\|e_{y_2}\| \tag{66}$$

$$\leq \|e_{y_2}\|(\|\phi\| + \|N_2\|\|\dot{f}\| - \mathcal{K}(t)), \tag{67}$$

where $\|\phi\|$ satisfies (62). Thus by choice of $\mathcal{K}(t)$ in (63) it follows

$$e^T_{y_2}\dot{e}_{y_2} \leq -\eta\|e_{y_2}\|$$

and a sliding motion is guaranteed in finite time. ∎

Remark 6. The modulation gain in (63) depends on knowledge on the bounds of d, f, and $\dot{f}$. Consequently the choice of $\mathcal{K}(t)$ requires a certain level of engineering judgment, knowledge and understanding of the system for which the monitoring scheme is being designed. To remove the assumption that bounds on d, f and $\dot{f}$ need to be known, adaptive schemes can be used. A recent possible choice is the "dual-layer" approach.[49]

The observer discussed in this section will now be applied to the problem of reconstruction of a yaw rate sensor fault associated with the MuPAL-α aircraft.

3 | AIL TEST ON THE MuPAL-α PLATFORM

3.1 | MuPAL-α platform

The MuPAL-α Aircraft-in-the-loop (AIL) platform[50] is currently used by the Japan Aerospace Exploration Agency to validate the performance of user-defined advanced guidance and control laws and FDD/FTC methodologies for both ground AIL tests inside the hanger (see Figure 1),[51,52] and actual flight tests including Simple Adaptive Control,[53] $\mathcal{H}_\infty$ Control,[23,54-57] Sliding Mode Control (SMC)[11,44] and an Indirect Adaptive Control strategy involving online parameter estimation.[58]

The schematic of the configuration of the MuPAL-α AIL test platform is shown in Figure 1A. Clearly, this configuration is different from the traditional flight simulator and it includes onboard actuators as components of the loop. Clearly from Figure 1A, a Fly-By-Wire (FBW) system is involved in the AIL schematic, which allows advanced flight control laws and validation scenarios to be created flexibly by the users. Figure 1A also includes an emulation computer which contains a high-fidelity aircraft motion model (typically of the Dornier aircraft motion model itself). Hence the model outputs (the aircraft's position and attitude), can be obtained from the emulation computer, and the outputs and the actual control surface deflections are used by the FBW computer to update the controller command, the cockpit displays and the outside view on the graphic display screen located outside the cockpit (see Figure 1D). All the control surfaces respond to the signals sent from the FBW system, and the actual position of the surfaces are used as inputs into the aircraft motion model in the emulation computer.

According to JAXA's protocols, all user-defined flight control laws are written in C-code which contains both the logic of the flight control law and the interface between the flight control and the FBW system. After the compilation, the codes

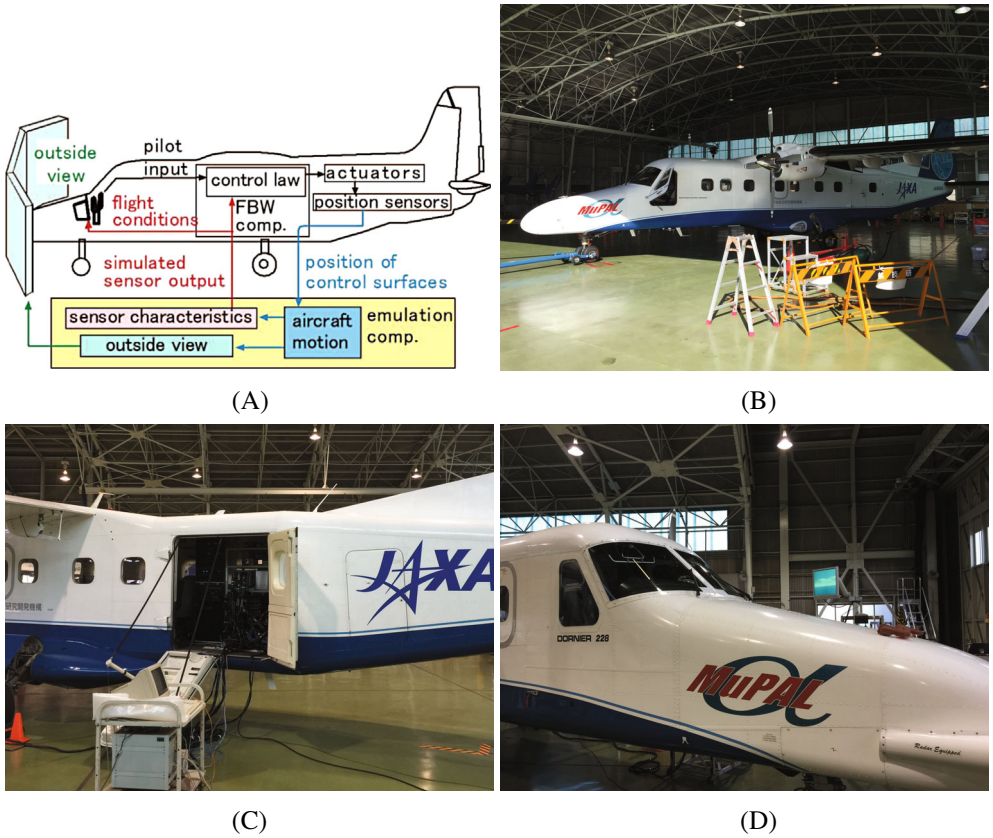

FIGURE 1 MuPAL-α AIL test platform. (A) AIL configuration, (B) aircraft in hanger, (C) "umbilical cords", (D) monitor for outside view for pilot

are "burned" into the FBW computer. The "flight data" obtained from the AIL is recorded for the purpose of performance analysis.

3.2 | Observer design results

This article specifically focuses on the aircraft's lateral-directional dynamics. The scheduling parameters are chosen as

$$\rho = \begin{bmatrix} v_{eas} & v_{eas}^2 \end{bmatrix}, \tag{68}$$

where v_{eas} represents the equivalent airspeed.[56] Because the regulatory constraints in JAXA mean most test flights are conducted at similar altitudes with almost identical mass and center of gravity positions. The scheduling parameters are v_{eas} and its square. Here the conservative assumption that $\rho_1(= v_{eas})$ and $\rho_2(= v_{eas}^2)$ are independent of each other was made and they are normalized to lie in the interval [0 1]. The LPV system and input matrices are provided in Appendix B.

The system states of the LPV model are given by

$$x = \begin{bmatrix} \phi & \beta & p & r \end{bmatrix}^T \tag{69}$$

which denote roll angle, sideslip angle, roll rate and yaw rate, respectively. Here it is assumed that the system outputs are

$$y = \begin{bmatrix} \phi & p & r \end{bmatrix}^T \tag{70}$$

and therefore

$$C = \begin{bmatrix} 1 & 0 & 0 & 0 \\ 0 & 0 & 1 & 0 \\ 0 & 0 & 0 & 1 \end{bmatrix}. \tag{71}$$

The system inputs for the purpose of these tests are

$$u = \begin{bmatrix} \delta_a & \delta_r \end{bmatrix}^T, \tag{72}$$

where δ_a and δ_r represent deflections of the aileron and the rudder. Consequently, in this example, $n = 4, p = 3$, and $q = 1$. Since only the yaw rate measurement is assumed to be corrupted by faults, the fault distribution matrix $F(\rho) = 0$ and

$$N = \begin{bmatrix} 0 & 0 & 1 \end{bmatrix}^T. \tag{73}$$

The disturbance distribution matrix $M(\rho)$ is assumed to be fixed and to take the form

$$M(\rho) = \begin{bmatrix} 0_{2\times 2} & I_2 \end{bmatrix}^T \tag{74}$$

which captures the effect of external disturbances such as wind and gusts impacting on the roll rate and yaw rate channels.

The design freedom in (55) are chosen as $W_1 = 0.1$ and $W_2 = 0.5I_3$. From Assumption 2, the LMIs in (55) and (57) are affine with respect to ρ and they can be synthesized using the SEDUMI solver with YALMIP parser. The weightings are chosen as $\alpha_1 = 0.2$ and $\alpha_2 = 0.8$, which gives a higher priority to the disturbance rejection. The observer gains $G_1(\rho)$ and $G_2(\rho)$ are in the form of

$$G_1(\rho) = G_{1,0} + G_{1,1}\rho_1 + G_{1,2}\rho_2 \quad \text{and} \quad G_2(\rho) = G_{2,0} + G_{2,1}\rho_1 + G_{2,2}\rho_2 \tag{75}$$

and their individual components are

$$G_{1,0} = \begin{bmatrix} -25.6336 & -3.4727 \\ 20.0000 & -40.0000 \\ 28.5935 & -0.0000 \\ 0 & 0 \end{bmatrix} \quad G_{1,1} = \begin{bmatrix} -11.0614 & 5.0103 \\ 0.0000 & 0.0000 \\ -13.0727 & -0.0000 \\ 0 & 0 \end{bmatrix} \quad G_{1,2} = \begin{bmatrix} 63.6898 & -3.3304 \\ -0.0000 & -0.0000 \\ 122.3122 & 0.0000 \\ 0 & 0 \end{bmatrix}, \tag{76}$$

$$G_{2,0} = \begin{bmatrix} 20.0185 \\ -2.9217 \\ -5.2010 \\ -2.7776 \end{bmatrix} \quad G_{2,1} = \begin{bmatrix} 3.3550 \\ 12.3238 \\ 41.2649 \\ 6.9181 \end{bmatrix} \quad G_{2,2} = \begin{bmatrix} -1.4794 \\ -9.3756 \\ 38.9927 \\ -51.4221 \end{bmatrix}. \tag{77}$$

In this design, the values of L are

$$L = \begin{bmatrix} 0 & 1.0441 & -0.4705 \end{bmatrix} \tag{78}$$

which ensures that $\bar{A}_{11}(\rho)$ is quadratically stable. The tuning matrix $\breve{A}^*_{22} = -0.1$ and the modulation gain $\mathcal{K}$ is chosen as 0.2. For safety reasons, it was determined that the magnitude of the sensor faults would be less that 5 deg/s. This is the maximum level of sensor faults typically tested during a flight evaluation campaign.[56] The magnitude of wind/gusts is assumed to be less than 4 m/s (This is also typical of the sort of conditions which may be encountered during flight testing.). Since $\rho(t)$ is bounded in a known compact set, the values of m_1, m_2, and m_3 in (62) can be estimated from (60) and (61). Then the initial modulation gain is chosen to ensure a sliding motion. The final value of

$\mathcal{K}(\cdot)$ was decided upon following extensive pre-flight ground testing on the MuPAL-α aircraft configured in an AIL setup.

The next section describes the implementation and testing of the observer scheme on JAXA's AIL.

3.3 | AIL test results

During the AIL tests, the flaps and gear are set to up in the emulation model, and the Direct Lift Control (DLC) FLAPS are fixed at 0 deg. The AIL test results in the following subsections are associated with a selected flight condition in which the mass of the aircraft is 5700 kg, the center of gravity is at 28%, the trim altitude is maintained at 5000 ft and the trimmed indicated airspeed is around 120 kts. The baseline controller, taken from Reference 44, is used to ensure good sideslip and roll angle tracking performance. During the AIL tests, the sideslip and roll angle commands are Autopilot commands. During the AIL tests, the yaw rate sensor measurement is corrupted by faults created at a software level. The faults which will be explored are typical of those used to test the efficacy of FDI schemes in the aerospace community.[4] In Reference 59, the particular SMO was benchmarked against several metrics including false alarms, miss detections and fault detection times, and so forth

3.3.1 | Fault free without wind/gust

First the results from a fault free AIL test without wind/gusts are shown in Figure 2. This scenario is used to provide a performance benchmark. An "S-turn" manoeuvre was created by the Auto-pilot and the response of the lateral directional states are shown in Figure 2A. Figure 2A demonstrates that sideslip and roll angle tracking performance is good. The corresponding aileron and rudder deflections are plotted in Figure 2B. Next, the nominal observer performance is shown in Figure 2C. In this baseline test, Figure 2C (bottom left) demonstrates the fault reconstruction error. For the majority of the test the error was in the bound ± 0.25 deg/s. Clearly there is correlation between the loss of accuracy in terms of fault estimation and the times at which the manoeuvres are initialized and finished. The worst case deviations in accuracy are all between ± 0.5 deg/s (Figure 9A). Figure 2C also shows sliding is maintained throughout. Though the comparisons between the histogram in the fault free case (see Figure 9A) with those in faulty cases, it will be seen that the best possible level of performance is obtained in this scenario since there are no wind and gust disturbances injected—although there are still un-modeled effects impacting on the results because of the hardware in the loop (the control surface actuator dynamics considered in Reference 56 have been ignored, there is latency in the communication etc).

Remark 7. To avoid false alarms, a simple thresh-holding approach would require a bound of at least ± 0.5 to be utilized. This would be the main factor in determining the detection times. Of course more sophisticated thresh-holding mechanisms can be employed—see for example the adaptive scheme used in conjunction with the SMO in Reference 59.

3.3.2 | Faulty cases—Sine wave

Figures 3 and 4 show the AIL evaluation results when an additive sine wave fault occurs on the yaw rate sensor from 30 s onwards. During this set of AIL tests, wind/gusts have been injected, but the same manoeuvre as the one created in the fault free scenario has been considered. The results obtained from two different sine wave faults are shown in this subsection. One sine wave fault signal has a frequency of 0.05 Hz and the other one has a frequency of 0.5 Hz. The amplitude of the two sine waves is 5 deg. In principle the low frequency one should be reconstructed more accurately and should not display any visible phase lag in the reconstruction. Figures 3 and 4 (top left) show that the additive sine wave faults appear in the yaw rate sensor measurements from 30 s onwards. Both faults can be accurately reconstructed (Figures 3 and 4 top right) and in both situations sliding is maintained (Figures 3 and 4 bottom left and right). Again in Figure 3 (and Figure 4) there is correlation between loss of accuracy, and the start/end of the manoeuvres. For most of the test time, the reconstruction errors lie between ± 0.5 deg/s although there are a couple of deviations outside this bound. The standard deviation of the error plots for this test is larger than the one associated with the fault free case (Figure 9C). In Figure 4, the reconstruction error lies mostly within the ± 0.5 deg/s bound as in the case with the lower frequency sine wave fault. The error signal in this case contains higher frequency components compared with the lower frequency

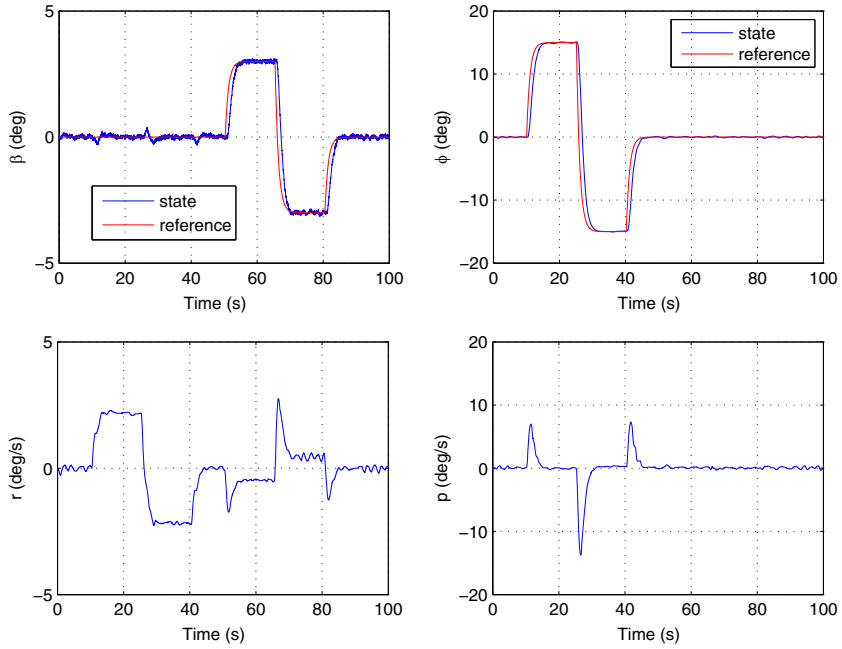

(A)

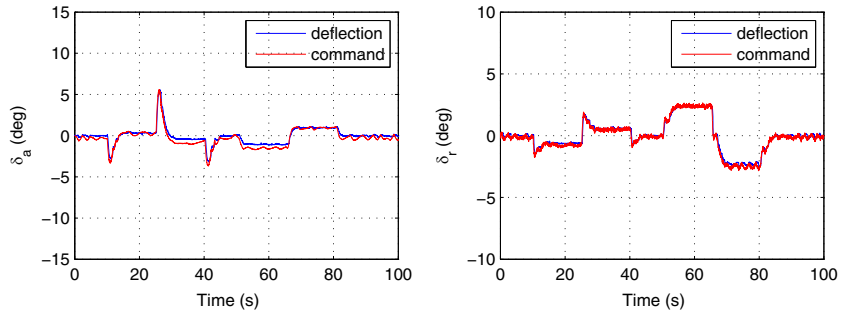

(B)

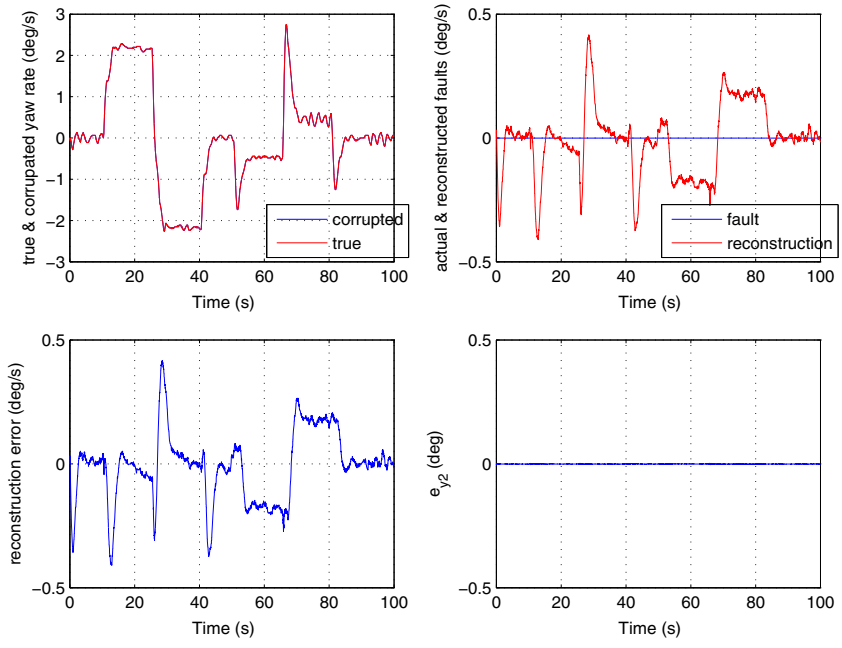

(C)

FIGURE 2 Fault-free case, no wind/gust. (A) The trajectories of the system states, (B) control surface deflections, (C) fault reconstruction performance

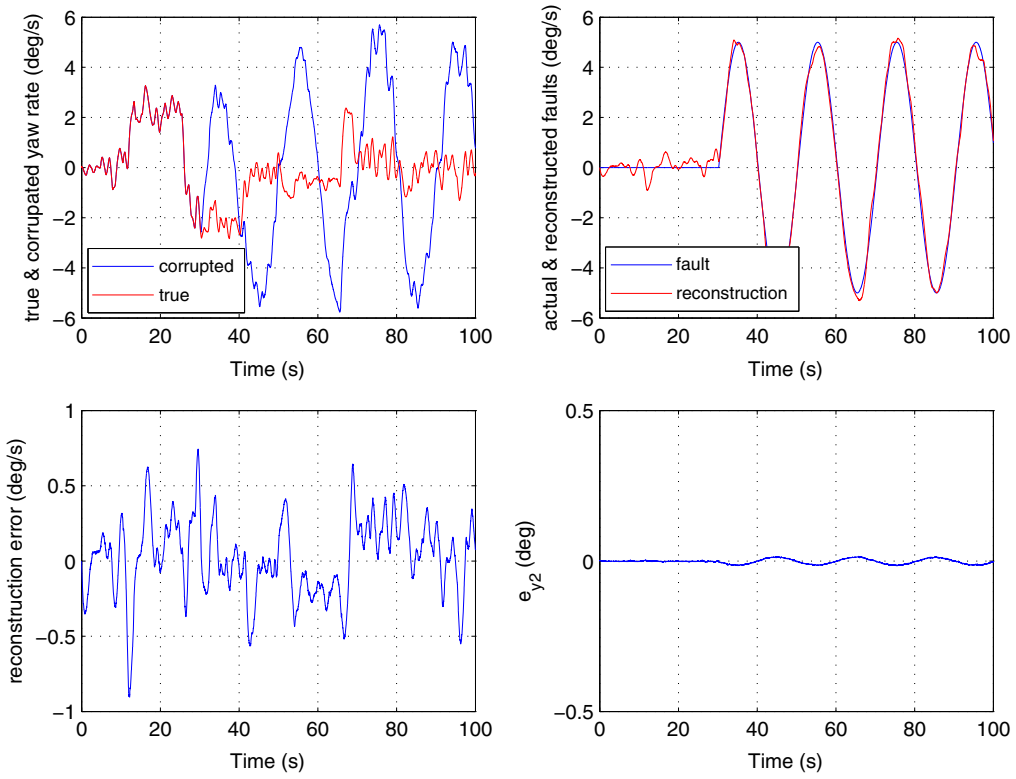

FIGURE 3 Faulty case, sine wave (frequency–0.05), wind/gust

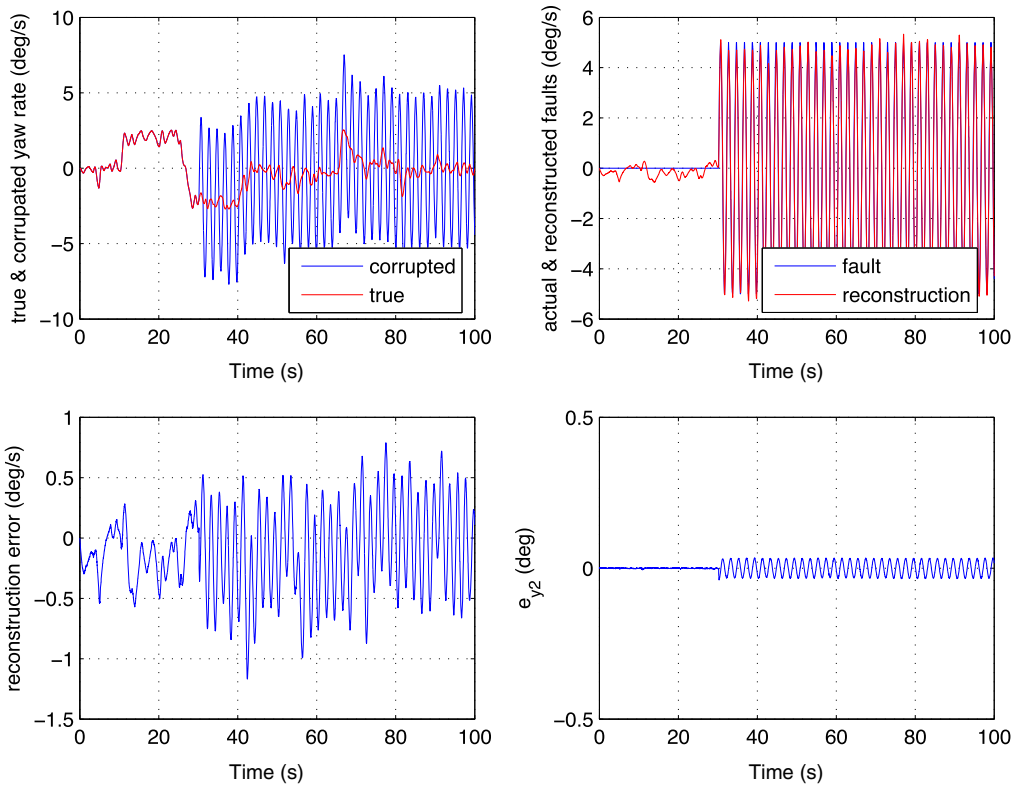

FIGURE 4 Faulty case, fast sine waves (frequency–0.5), wind/gust

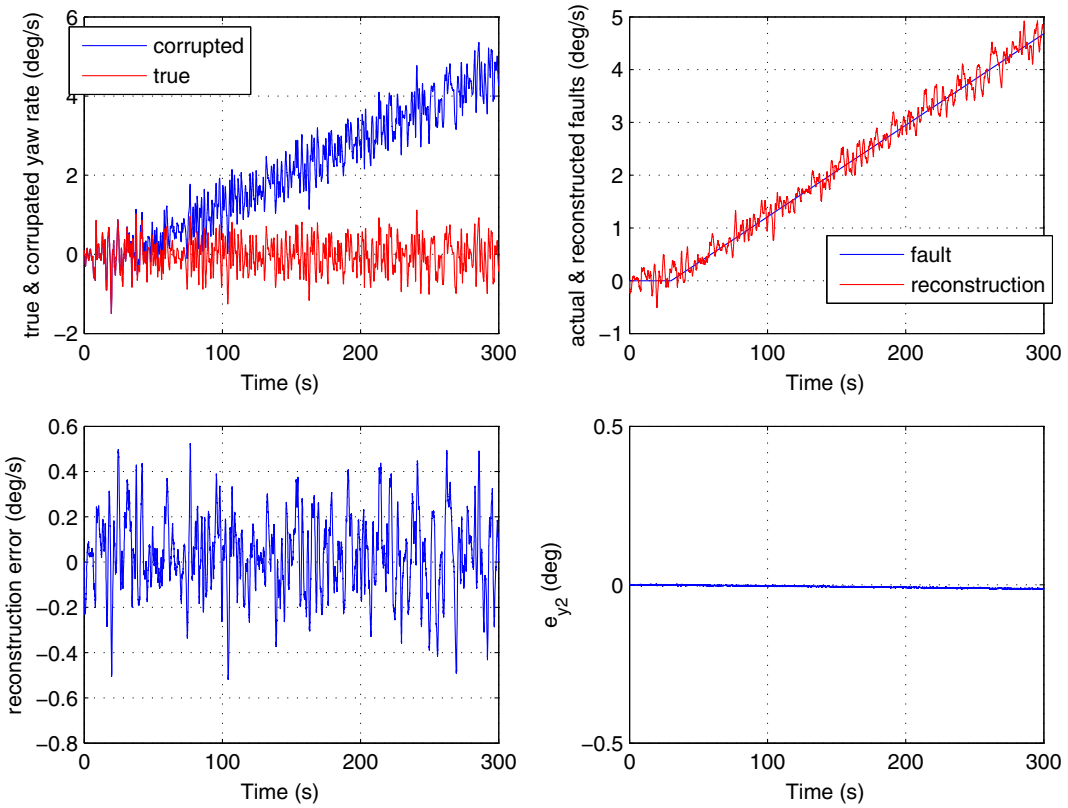

FIGURE 5 Faulty case, slow drift, wind/gust, long run, no maneuver

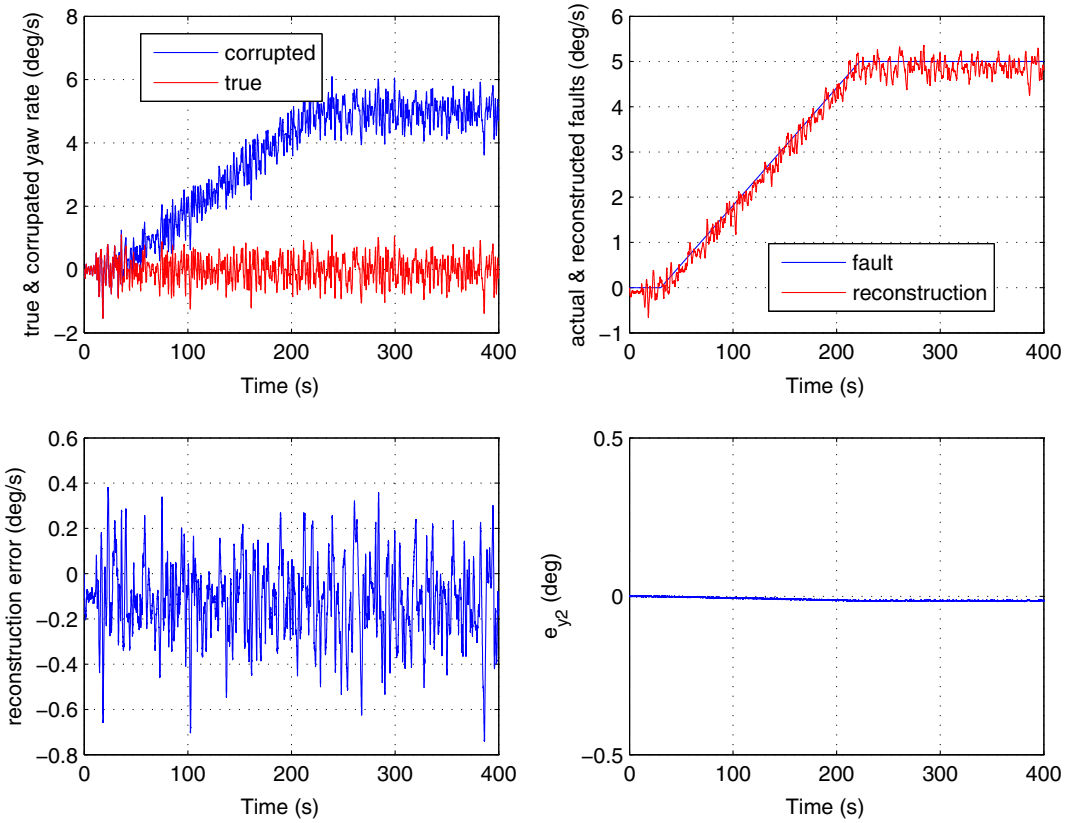

FIGURE 6 Faulty case, fast drift, wind/gust, long run, no maneuver

sine wave, and the standard deviation is slightly larger (Figure 9C). This is perhaps to be expected because this is a more challenging situation compared to the lower frequency sine wave faulty case.

3.3.3 | Faulty cases—Drift

Next, results (in the presence of wind/gusts) are shown when drift faults occur on the yaw rate sensor from 30 s onwards. Both a slow drift (with a rate of 0.017 deg /s^2) and a fast drift rate (0.025 deg /s^2) are considered as shown in Figures 5 and 6. During this set of AIL tests, no manoeuvre was created, but the testing period was increased to 5mins. The results correspond to the maximum allowable amplitude of fault which is permitted in actual flight tests.[11]

Clearly, although yaw rate sensor drifts are present, the fault estimation scheme can estimate the fault with a good level of precision. As shown in Figure 9D, the error distributions of both the drift scenarios are very similar to each other (and similar to the fault free case). The errors predominantly fall within the ±0.5 deg/s bound once more. Furthermore, Figures 5 and 6 (bottom right) show that sliding is maintained.

3.3.4 | Faulty cases—NRZ

Figure 7 is associated with a non-return-to-zero sensor fault which is commonly used by the aerospace industry to validate fault diagnosis performance in the face of discontinuous faults.[60] The fault is set to occur from 30 s onwards. The switching rate of the NRZ signal is chosen to be 0.5 Hz, and the amplitude set to be 2 deg. Here the same doublet manoeuvre created by the Auto-pilot is considered for consistency. Figure 7 (top right) shows the fault estimation performance. This is the most challenging case in some ways. Although the frequency of 0.5 Hz is the same as the fast sinusoid scenario—now the fault is non-differentiable at the transition points. Thus formally, this class of faults does not meet the assumption of

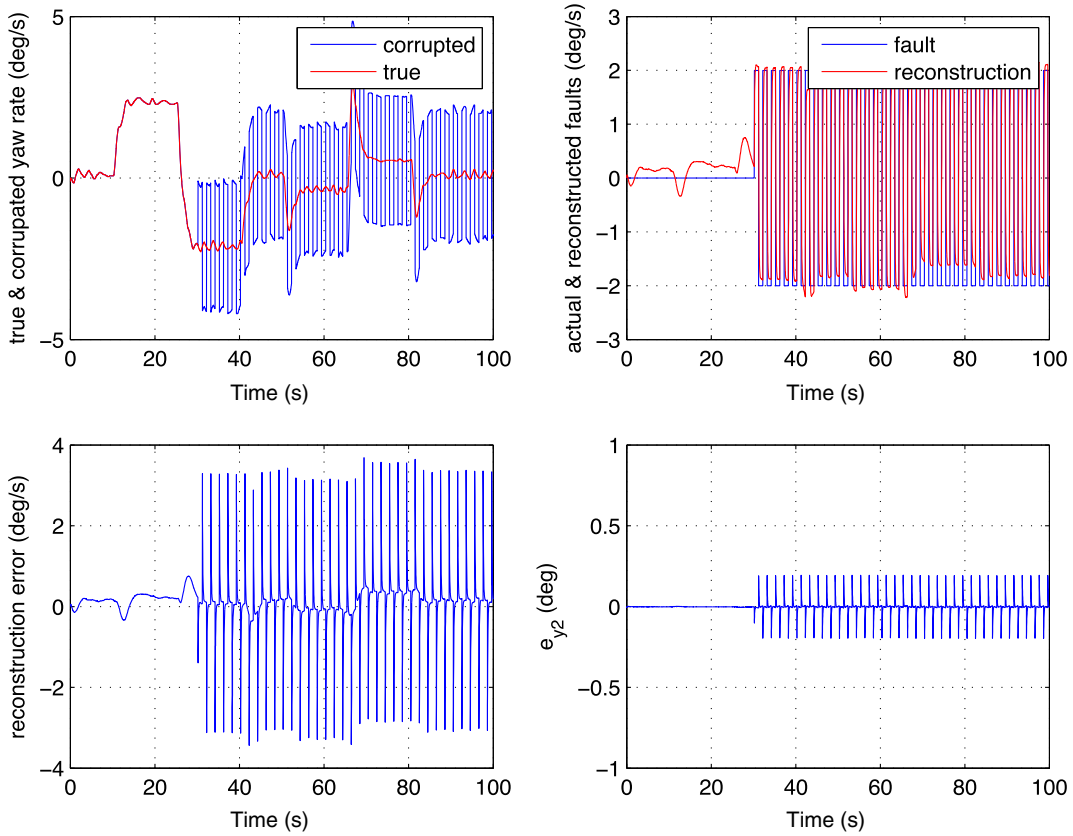

FIGURE 7 Faulty case, NRZ, frequency 0.5, NRZ magnitude 2 deg/s, no wind/gust

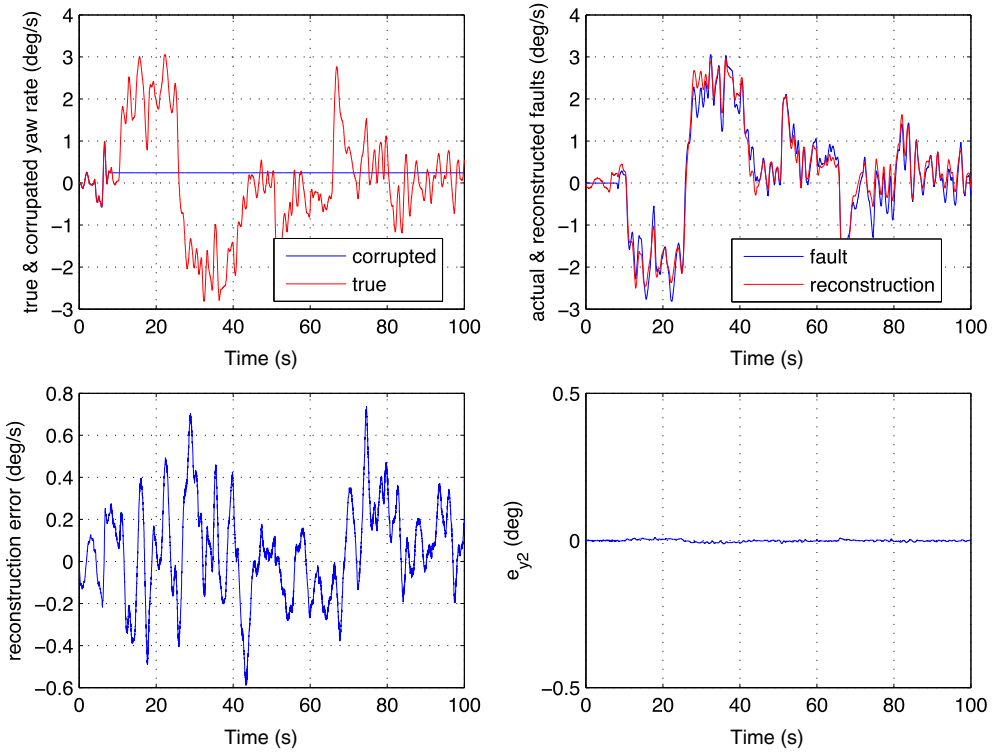

(A)

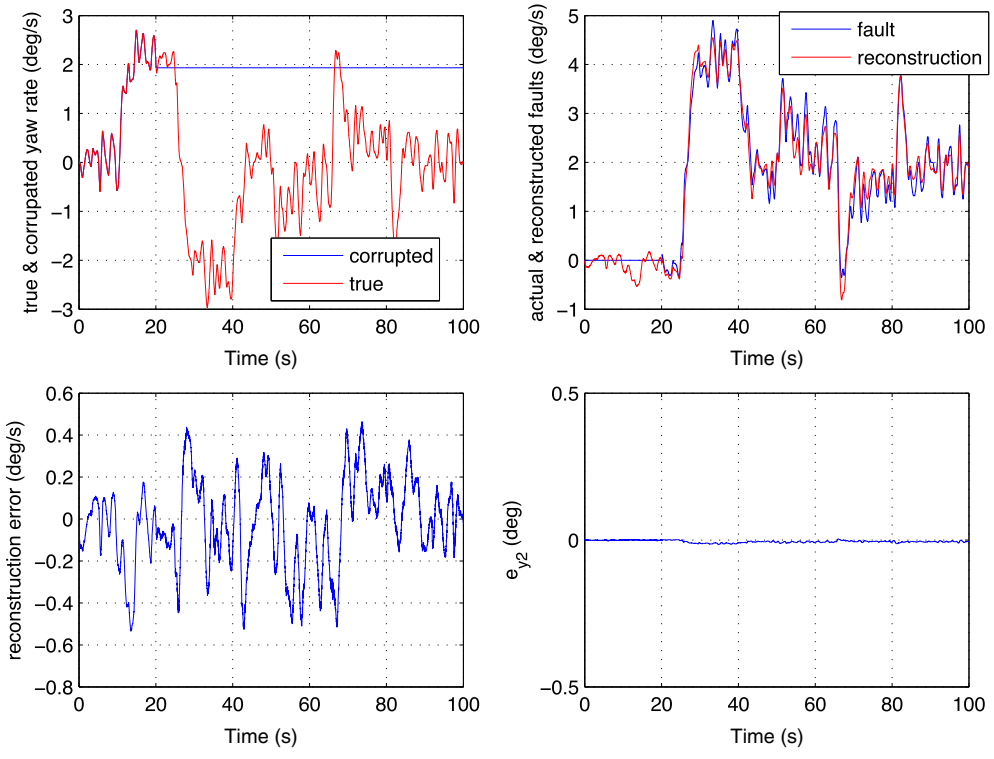

(B)

FIGURE 8 Faulty case, "lock-in-the-place", fault occurrence time (A) 8 s and (B) 20 s, wind/gust.

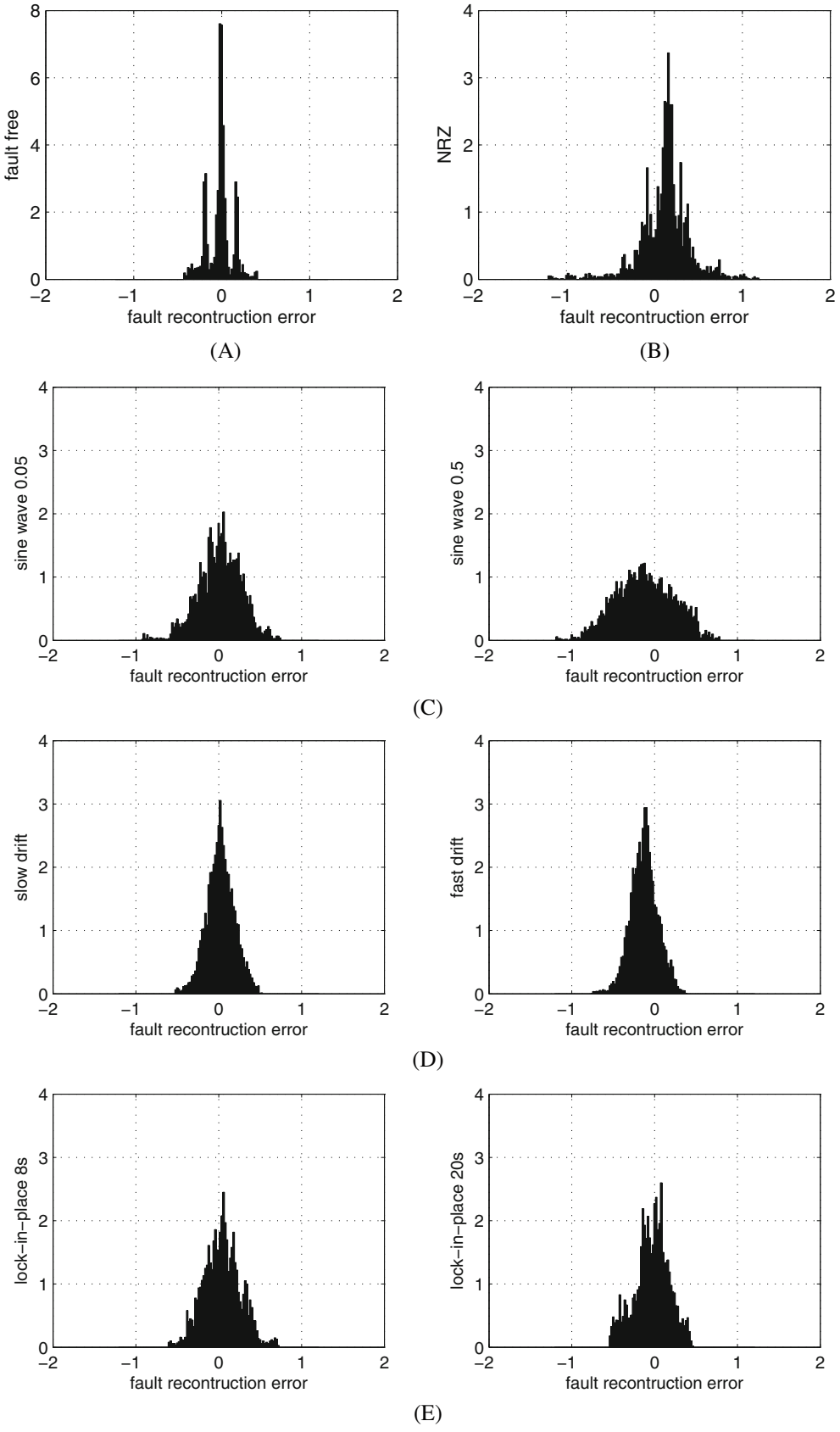

FIGURE 9 Normalized histogram. (A) Fault free case, (B) NRZ, (C) sine wave, (D) drift, (E) lock-in-the-place

TABLE 1 RMS values of the fault estimation errors

Validation scenarios	RMS
Fault free without wind/gust	0.1420
Sinewave – 0.05	0.2616
Sinewave – 0.5	0.3703
Slowdrift	0.1721
Fastdrift	0.2037
NRZ	0.6770
Lock in the place at 8 s	0.2291
Lock in the place at 20 s	0.2097

Section 2. However this fault is used within the aerospace community to test the efficacy of FDI schemes[4,59]. Crucially, the points of non-differentiably are isolated and countable, and manifest themselves as sharp peaks in the fault estimation errors occurring when, instantaneously, sliding is broken. Whilst most of the time the errors remain between ±0.5 rad/s there are more pronounced tails to both sides of the error distributions as shown in Figure 9B.

3.3.5 | Faulty cases—"Lock-in-the-place"

Figure 8 shows the AIL evaluation results, in the presence of wind/gusts, when a "lock-in-the-place" occurs on the yaw rate sensor. For consistency, the manoeuvre created by the Auto-pilot is same as those used in previous tests. Figure 8A,B show the results when a "lock-in-the-place" occurs at 8 and 20 s, respectively. It can be seen from Figure 8A,B that, after the fault occurs, the yaw rate sensor measurements are frozen at fixed values. From Figure 8A,B (top right and bottom left), it can be seen that the faults are reconstructed accurately in the presence of wind/gusts. The error distribution here (Figure 9D) is very similar to the fault free case with the errors lying between ±0.5deg/s. Furthermore, sliding can be maintained when the "lock-in-the-place" occurs (Figure 8A,B bottom right).

3.3.6 | RMS indices

Table 1 shows the performance indices of the proposed fault estimation scheme in the face of various fault scenarios. Here the root mean squared (RMS) values of the fault estimation errors are used to measure the precision of fault estimation. The relative size of the RMS values in Table 1 are consistent with the shape of histograms shown in Figure 9. The results largely accord with intuition. The poorest performance is associated with the NRZ fault—this is to be expected since formally this class of fault does not meet the differentiability requirements, and sliding is temporarily broken at times when the fault derivative does not exist. Best performance is achieved during a slow drift. Such an incipient fault is often difficult to detect until the level of fault exceeds a threshold above the typical levels of noise and disturbances experienced by the (fault free) systems. Sine wave faults are more challenging than drift faults to replicate and tend to expose lags in reconstruction. Also higher frequency sine waves are more challenging than lower frequency ones. These are borne out in the RMS values.

4 | CONCLUSIONS

This article has considered the problem of unknown input estimation in a system which has a linear parameter varying structure. The article has proposed a scheme, based on classical sliding mode ideas which creates a smooth estimate of the unknown input. Although the process may be viewed as a filtering of the discontinuous injection, there is no additional phase lag introduced in the process. A clear design strategy has been articulated and the problem has been

posed in terms of linear matrix inequalities: the objective is to minimize the $\mathcal{L}_2$ gain between the fault estimate and a class of external disturbance impacting on the system, whilst ensuring linear–quadratic regulator-like dynamics associated with the sliding motion. The proposed scheme was validated using the Japan Aerospace Exploration Agency's Multi-Purpose Aviation Laboratory (MuPAL-α) aircraft-in-the-loop platform. Some aircraft-in-the-loop validation results were presented to demonstrate the design efficacy. Future work could focus on the relaxation of the design conservatism via: (a) considering a parameter dependent Lyapunov matrix; (b) formulating the parameter dependent matrices $A(\rho)$, $F(\rho)$, and $M(\rho)$ in a more general way; and (c) addressing the robustness issue with respect to certain classes of parametric uncertainty.

ACKNOWLEDGMENT

This work was supported by the EU H2020 under grant agreement No. 690811 and the Japan NEDO under grant agreement No. 062800, as a part of the VISION project.

CONFLICT OF INTEREST

The authors declared that they have no conflict of interest to this work.

DATA AVAILABILITY STATEMENT

Research data are not shared.

ENDNOTES

*There is a much wider literature on the unknown input observer problem in which the aim is to robustly estimate the state and the unknown disturbance is to be rejected rather than estimated.

†Although in considering a (fixed) quadratic Lyapunov function is conservative, this assumption is fundamental to the developments in this section and is explicitly exploited to create a change of coordinates.

ORCID

Lejun Chen https://orcid.org/0000-0002-8078-0582
Christopher Edwards https://orcid.org/0000-0002-2222-0640
Halim Alwi https://orcid.org/0000-0002-2892-6660
Masayuki Sato https://orcid.org/0000-0003-0387-3467
Shamila Nateghi https://orcid.org/0000-0003-0967-0257
Yuri Shtessel https://orcid.org/0000-0003-4980-2621

REFERENCES

1. Marcos A, Balas GJ. Development of linear parameter-varying models for aircraft. *J Guid Control Dyn*. 2004;27:218-228.
2. Mohammadpour J, Scherer CW. *Control of Linear Parameter Varying Systems with Applications*. Springer; 2012.
3. Edwards C, Lombaerts T, Smaili H. *Fault Tolerant Flight Control: A Benchmark Challenge*. Springer; 2010.
4. Goupil P, Marcos A. The European ADDSAFE project: industrial and academic efforts towards advanced fault diagnosis. *Control Eng Pract*. 2014;31:109-125.
5. Goupil P, Dayre R, Brot P. From theory to flight tests: airbus flight control system TRL5 achievements. Proceedings of the IFAC World Congress; 2014.
6. Vanek B, Edelmayer A, Szabo Z, Bokor J. Bridging the gap between theory and practice in LPV fault detection for flight control actuators. *Control Eng Pract*. 2014;31:171-182.
7. Varga A, Goupil P, Marcos A. CEP special section issue on advanced fault diagnosis for sustainable flight control—The European ADDSAFE project. *Control Eng Pract*. 2014;31:107-108.
8. Chen J, Patton RJ. *Robust Model-Based Fault Diagnosis for Dynamic Systems*. Kluwer Academic Publishers; 1999.
9. Blanke M, Kinnaert M, Lunze J, Staroswiecki M. *Introduction to Diagnosis and Fault-Tolerant Control*. Springer; 2016.
10. Zhang Y, Jiang J. Bibliographical review on reconfigurable fault-tolerant control systems. *Annu Rev Control*. 2008;32:229-252.
11. Chen L, Alwi H, Edwards C, Sato M. Flight evaluation of an LPV sliding mode observer for sensor FTC. *IEEE Trans Control Syst Technol*. 2021. doi:10.1109/TCST.2021.3096946
12. Chen W, Yang J, Guo L, Li S. Disturbance-observer-based control and related methods—An overview. *IEEE Trans Ind Electron*. 2016;63:1083-1095.
13. Na J, Chen AS, Herrmann G, Burke R, Brace C. Vehicle engine torque estimation via unknown input observer and adaptive parameter estimation. *IEEE Trans Veh Technol*. 2018;67:409-422.
14. Nguyen T, Khan SG, Hatano T, et al. Real-time sliding mode observer scheme for shear force estimation in a transverse dynamic force microscope. *Asian J Control*. 2018;20:1317-1328.

15. Nateghi S, Shtessel Y, Edwards C, Barbot JP. Secure state estimation and attack reconstruction in cyber-physical systems: sliding mode observer approach. In: Volosencu C, Saghafinia A, Du X, Chakrabarty S, (eds). *Control Theory in Engineering*. IntechOpen; 2019:3.
16. Nateghi S, Shtessel Y, Edwards C. Resiliant control of cyber-physical systems under sensor and acutator attacks driven by adaptive sliding mode observers. *Int J Robust Nonlinear Control*. 2022.
17. Ljung L. Asymptotic behavior of the extended Kalman filter as a parameter estimator for linear systems. *IEEE Trans Automat Contr*. 1979;24:36-50.
18. Gheorghe A, Zolghadri A, Cieslak J, Goupil P, Dayre R, Le Berre H. Model-based approaches for fast and robust fault detection in an aircraft control surface servo loop: from theory to flight tests [applications of control]. In: Bordeneuve-Guibé J, Drouin A, Roos C, (eds.) *IEEE Control Syst Mag*. 2013;33:20-84.
19. Corless M, Tu J. State and input estimation for a class of uncertain systems. *Automatica*. 1998;34:757-764.
20. Walcott BL, Corless MJ, Zak SH. Comparative study of non-linear state-observation techniques. *Int J Control*. 1987;45:2109-2132.
21. Stoustrup J, Niemann HH. Fault estimation – A standard problem approach. *Int J Robust Nonlinear Control*. 2002;12:649-673.
22. Edwards C, Spurgeon SK, Patton RJ. Sliding mode observers for fault detection and isolation. *Automatica*. 2000;36:541-553.
23. Sato M, Akasaka D. Luenberger observer-based flight controller design using robust control toolbox™. Proceedings of the IEEE Conference on Control Technology and Applications; 2021:1160-1165.
24. Khalil H, Praly L. High-gain observers in nonlinear feedback control. *Int J Robust Nonlinear Control*. 2010;24:993-1015.
25. Ellero N, Gucik-Derigny D, Henry D. An unknown input interval observer for LPV systems under L_2-gain and L_∞-gain criteria. *Automatica*. 2019;103:294-301.
26. Marx B, Ichalal D, Ragot J, Maquin D, Mammar S. Unknown input observer for LPV systems. *Automatica*. 2019;100:67-74.
27. Hammouri H, Tmar Z. Unknown input observer for state affine systems: a necessary and sufficient condition. *Automatica*. 2010;46(2):271-278.
28. Edwards C, Spurgeon SK. A sliding mode observer based FDI scheme for the ship benchmark. *Eur J Control*. 2000;6:341-355.
29. Tan C, Edwards C. Sliding mode observers for detection and reconstruction of sensor faults. *Automatica*. 2002;38:1816-1821.
30. Alwi H, Edwards C, Tan CP. *Fault Detection and Fault-Tolerant Control Using Sliding Modes*. Springer; 2011.
31. Edwards C, Spurgeon SK. *Sliding Mode Control: Theory and Applications*. Taylor & Francis; 1998.
32. Levant A. Robust exact differentiation via sliding mode technique. *Automatica*. 1998;34:379-384.
33. Fridman L, Levant A, Davila J. Observation of linear systems with unknown inputs via high-order sliding-modes. *Int J Syst Sci*. 2007;38:773-791.
34. Fridman L, Shtessel Y, Edwards C, Yan XG. Higher-order sliding-mode observer for state estimation and input reconstruction in nonlinear systems. *Int J Robust Nonlinear Control*. 2008;18:399-412.
35. Falcón R, Ríos H, Dzul A. A robust fault diagnosis for quad-rotors: a sliding-mode observer approach. *IEEE/ASME Trans Mechatron*. 2022. doi:10.1109/TMECH.2022.3156854
36. Ríos H, Davila J, Fridman L, Edwards C. Fault detection and isolation for nonlinear systems via high-order-sliding-mode multiple-observer. *Int J Robust Nonlinear Control*. 2015;25:2871-2893.
37. Pérez U, Capello E, Punta E, Perea J, Fridman L. Fault detection and isolation for a 3-dof helicopter with sliding mode strategies. Proceedings of the 15th International Workshop on Variable Structure Systems (VSS); 2018:279-284.
38. Cieslak J, Ferreira de Loza A, Henry D, Davila J, Zolghadri A. Sliding mode observers for fault estimation in multisensor avionics systems. In: Bordeneuve-Guibé J, Drouin A, Roos C, (eds). *Advances in Aerospace Guidance, Navigation and Control*. Springer International Publishing; 2015:323-342.
39. Utkin V. *Sliding Modes in Control and Optimization*. Springer; 1992.
40. Sato M. One-shot design of performance scaling matrices and observer-based gain-scheduled controllers depending on inexact scheduling parameters. *Syst Control Lett*. 2020;137.
41. Chen L, Edwards C, Alwi H. Sensor fault estimation using LPV sliding mode observers with erroneous scheduling parameters. *Automatica*. 2019;101:66-77.
42. Chandra KPB, Alwi H, Edwards C. Fault detection in uncertain LPV systems with imperfect scheduling parameter using sliding mode observers. *Eur J Control*. 2017;34:1-15.
43. Chen L, Alwi H, Edwards C. On the synthesis of an integrated active LPV FTC scheme using sliding modes. *Automatica*. 2019;110:108536.
44. Chen L, Alwi H, Edwards C, Sato M. Flight evaluation of a sliding mode online control allocation scheme for fault tolerant control. *Automatica*. 2020;114.
45. Apkarian P, Gahinet P, Becker G. Self-scheduled H_∞ control of linear parameter-varying systems: a design example. *Automatica*. 1995;31:1251-1261.
46. Rosa P, Balas GJ, Silvestre C, Athans M. A synthesis method of LTI MIMO robust controllers for uncertain LPV plants. *IEEE Trans Automat Contr*. 2014;59:2234-2240.
47. Packard AK. Gain scheduling via linear fractional transformations. *Syst Control Lett*. 1994;22:79-92.
48. Apkarian P, Gahinet P. A convex characterization of gain-scheduled H_∞ controllers. *IEEE Trans Automat Contr*. 1995;40:853-864.
49. Edwards C, Shtessel YB. Adaptive continuous higher order sliding mode control. *Automatica*. 2016;65:183-190.
50. Masui K, Tsukano Y. Development of a new in-flight simulator MuPAL-α. Modeling and Simulation Technologies Conference; 2000:4574; AIAA Paper.
51. Waitman S, Marcos A, Sato M. Design and hardware-in-the-loop validation of a fault-tolerant Y* flight control law. *Systol*. 2019:177-182.
52. Chen L, Edwards C, Alwi H, Sato M. Hardware-in-the-loop simulation for a sliding mode FDI scheme. Proceedings of the American Control Conference; 2019:4436-4441.

53. Matsuki H, Nishiyama T, Omori Y, Suzuki S, Masui K, Sato M. Flight test of fault-tolerant flight control system using simple adaptive control with PID controller. *Aircr Eng Aerosp Technol*. 2018;90:210-218.
54. Sato M, Satoh A. Flight control experiment of multipurpose-aviation-laboratory-α in-flight simulator. *J Guid Control Dyn*. 2011;34:1081-1096.
55. Marcos A, Waitman S, Sato M. Fault tolerant linear parametervarying flight control design, verification and validation. *J Franklin Inst*. 2022;359:653-676.
56. Sato M. Robust gain-scheduled flight controller for an in-flight simulator. *IEEE Trans Aerosp Electron Syst*. 2020;56:2122-2135.
57. Sato M, Peaucelle D. Conservatism reduction for LPV control design facing inexact scheduling parameters illustrated on flight tests. *Int J Robust Nonlinear Control*. 2020;30:6130-6148.
58. Hardier G, Ferreres G, Sato M. Design and flight testing of an adaptive gain-scheduled controller using on-line model estimation. *IEEE CCTA*. 2018;766-773.
59. Alwi H, Edwards C. Development and application of sliding mode LPV fault reconstruction schemes for the ADDSAFE Benchmark. *Control Eng Pract*. 2014;31:148-170.
60. Goupil P, Boada-Bauxell J, Marcos A, Rosa P, Kerr M, Dalbies L. An overview of the FP7 RECONFIGURE project: industrial, scientific and technological objectives. *IFAC-PapersOnLine*. 2015;48:976-981.

How to cite this article: Chen L, Edwards C, Alwi H, Sato M, Nateghi S, Shtessel Y. Sliding mode observers for robust fault estimation in linear parameter varying systems. *Int J Robust Nonlinear Control*. 2022;1-25. doi: 10.1002/rnc.6307

APPENDIX A

Let A_ρ and F_ρ represent the system and fault distribution matrices $A(\rho)$ and $F(\rho)$ frozen at a particular value of ρ. Then this appendix shows that for the LTI system (A_ρ, F_ρ, C_1, N)

$$(A_\rho - F_\rho N_2^{-1} C_2, C_1) \text{ is } \textit{detectable} \Leftrightarrow (A_\rho, F_\rho, C, N) \text{ has stable invariant zeros.} \tag{A1}$$

Consider a Rosenbrock system matrix given by

$$R(s) = \begin{bmatrix} sI - A_\rho & F_\rho \\ -C & N \end{bmatrix}. \tag{A2}$$

Then (A_ρ, F_ρ, C, N) has stable invariant zeros if and only if $R(s)$ has full column rank for all $s \in \mathbb{C}_+$.

Exploiting the structure of C and N, (A2) can be written as

$$R(s) = \begin{bmatrix} sI - A_\rho & F_\rho \\ -C_1 & 0 \\ -C_2 & N_2 \end{bmatrix}. \tag{A3}$$

For the case when $R(s)$ has the form in (A3), $R(s)$ has full column rank if and only if

$$R(s) \begin{bmatrix} \eta_1 \\ \eta_2 \end{bmatrix} = 0 \tag{A4}$$

implies $\eta_1 = 0$ and $\eta_2 = 0$ where $\eta_1 \in \mathbb{R}^n$ and $\eta_2 \in \mathbb{R}^q$. Equation (A4) is equivalent to

$$(sI - A_\rho)\eta_1 + F_\rho \eta_2 = 0, \tag{A5}$$
$$-C_1 \eta_1 = 0, \tag{A5}$$
$$-C_2 \eta_1 + N_2 \eta_2 = 0, \tag{A5}$$

and since N_2 is square and invertible, (A7) is equivalent to $\eta_2 = N_2^{-1}C_2\eta_1$. Therefore

$$R(s)\begin{bmatrix}\eta_1\\ \eta_2\end{bmatrix} = 0 \quad \Leftrightarrow \quad (sI - A_\rho)\eta_1 + F_\rho N_2^{-1}C_2\eta_1 = 0 \ \text{ and } \ -C_1\eta_1 = 0. \tag{A8}$$

Thus $R(s)$ has full column rank for all $s \in \mathbb{C}_+$ if and only if

$$\begin{bmatrix} sI - A_\rho + F_\rho N_2^{-1}C_2 \\ -C_1 \end{bmatrix}\eta_1 = 0 \tag{A9}$$

implies $\eta_1 = 0$ for all $s \in \mathbb{C}_+$. From the Popov–Belevitch–Hautus test, this is equivalent to $(A_\rho - F_\rho N_2^{-1}C_2, C_1)$ being detectable.

Remark 8. The condition that the $(A_\rho - F_\rho N_2^{-1}C_2, C_1)$ needs to be detectable is identical to the conditions which would be required if the SMO approach adopted in Reference 11 was employed to address the fault estimation problem in (1).

APPENDIX B

The constant matrices used to construct $A(\rho)$ and $B(\rho)$ are given by

$$A_{p,0} = \begin{bmatrix} 0.0000 & -0.0000 & 1.0000 & 0.1461 \\ 0.1736 & -0.1418 & 0.1417 & -0.9813 \\ 0.0000 & -2.5507 & -3.2335 & 1.4601 \\ -0.0000 & 0.8983 & -0.1603 & -0.3838 \end{bmatrix}, \quad A_{p,1} = \begin{bmatrix} -0.0000 & -0.0000 & 0.0000 & -0.6162 \\ -0.2505 & -0.2108 & -0.5996 & -0.0686 \\ 0.0000 & -1.8764 & -2.6128 & -1.1804 \\ -0.0000 & 0.4195 & 0.8070 & -0.5433 \end{bmatrix},$$

$$A_{p,1} = \begin{bmatrix} 0.0000 & 0.0000 & -0.0000 & 0.4688 \\ 0.1665 & 0.0300 & 0.4547 & 0.0599 \\ -0.0000 & -6.2290 & -0.3881 & 0.9811 \\ 0.0000 & 5.2238 & -0.4142 & 0.1133 \end{bmatrix}, \quad B_{p,0} = \begin{bmatrix} -0.0000 & -0.0000 \\ 0.0000 & 0.0361 \\ -7.5828 & 0.8352 \\ 0.1863 & -1.5380 \end{bmatrix}, \quad B_{p,1} = \begin{bmatrix} 0.0000 & 0.0000 \\ 0.0000 & 0.0367 \\ 0.3087 & -0.0275 \\ 0.0107 & 0.0780 \end{bmatrix},$$

$$B_{p,2} = \begin{bmatrix} -0.0000 & -0.0000 \\ 0.0000 & -0.0005 \\ -21.7832 & 2.4224 \\ 1.0708 & -4.7836 \end{bmatrix}. \tag{B1}$$